A 5MW direct-drive generator for floating spar-buoy wind turbine: Drive-train dynamics

Journal:	*Part C: Journal of Mechanical Engineering Science*
Manuscript ID	JMES-14-0900.R2
Manuscript Type:	Original article
Date Submitted by the Author:	n/a
Complete List of Authors:	Sethuraman, Latha; University of Edinburgh, Institute for Energy Systems Xing, Yihan; Norwegian University of Science and Technology, Department of Marine Technology Venugopal, Vengatesan; University of Edinburgh, Institute for Energy Systems Gao, Zhen; Norwegian University of Science and Technology, Department of Marine Technology Mueller, Markus; University of Edinburgh, Institute for Energy Systems Moan, Torgeir; Norwegian University of Science and Technology, Department of Marine Technology
Keywords:	Floating wind turbine, direct-drive generator, Multi-body simulation, Eccentricity, Unbalanced Magnetic pull, bearing load
Abstract:	This article proceeds with investigations on a 5MW direct-drive floating wind turbine system (FWTDD) that was developed in a previous study. A fully integrated land-based direct drive wind turbine system (WTDD) was created using SIMPACK, a multi-body simulation tool, to model the necessary response variables. The comparison of blade pitch control action and torque behavior with a similar land-based direct-drive model in HAWC2 (an aero-elastic simulation tool) confirmed that the dynamic feedback effects can be ignored. The main shaft displacements, air-gap eccentricity, forces due to unbalanced magnetic pull (UMP) and the main bearing loads were identified as the main response variables. The investigations then proceed with a 2-step de-coupled approach for the detailed drive-train analysis in WTDD and FWTDD systems. The global motion responses and drive-train loads were extracted from HAWC2 and fed to stand-alone direct-drive generator models in SIMPACK. The main response variables of WTDD and FWTDD system were compared. The FWTDD drive-train was observed to endure additional excitations at wave and platform pitch frequencies, thereby increasing the axial components of loads and displacements. If secondary deflections are not considered, the FWTDD system did not result in any exceptional increases to eccentricity and UMP with the generator design tolerances being fairly preserved. The bearing loading behavior was comparable between both the systems, with the exception of axial loads and tilting moments attributed to additional excitations in the FWTDD system.

A 5MW direct-drive generator for floating spar-buoy wind turbine: Drive-train dynamics

Latha Sethuraman[1], *Yihan Xing*[2], *Vengatesan Venugopal*[1], *Zhen Gao*[2], *Markus Mueller*[1] *Torgeir Moan*[2]

[1] Institute for Energy Systems, The University of Edinburgh, Edinburgh, EH9 3JL, United Kingdom.

[2] Department of Marine Technology, Norwegian University of Science and Technology, 7491 Trondheim, Norway.

ABSTRACT

This article proceeds with investigations on a 5MW direct-drive floating wind turbine system (FWTDD) that was developed in a previous study. A fully integrated land-based direct drive wind turbine system (WTDD) was created using SIMPACK, a multi-body simulation tool, to model the necessary response variables. The comparison of blade pitch control action and torque behaviour with a similar land-based direct-drive model in HAWC2 (an aero-elastic simulation tool) confirmed that the dynamic feedback effects can be ignored. The main shaft displacements, air-gap eccentricity, forces due to unbalanced magnetic pull (UMP) and the main bearing loads were identified as the main response variables. The investigations then proceed with a 2-step de-coupled approach for the detailed drive-train analysis in WTDD and FWTDD systems. The global motion responses and drive-train loads were extracted from HAWC2 and fed to stand-alone direct-drive generator models in SIMPACK. The main response variables of WTDD and FWTDD system were compared. The FWTDD drive-train was observed to endure additional excitations at wave and platform pitch frequencies, thereby increasing the axial components of loads and displacements. If secondary deflections are not considered, the FWTDD system did not result in any exceptional increases to eccentricity and UMP with the generator design tolerances being fairly preserved. The bearing loading behaviour was comparable between both the systems, with the exception of axial loads and tilting moments attributed to additional excitations in the FWTDD system.

KEYWORDS

Floating wind turbine; direct-drive generator; Multi-body simulation; eccentricity; Unbalanced Magnetic pull; bearing load

Corresponding author

L.Sethuraman, Institute for Energy Systems, School of Engineering, The University of Edinburgh, The King's Buildings, Edinburgh, EH9 3JL, United Kingdom.
Email: *lssraman@gmail.com*

Abbreviations

BR	Bearing
CRB	Cylindrical Roller Bearing
FWT	Floating wind turbine
FWTDD	Floating wind turbine with direct-drive generator
PMG	Permanent Magnet Generator
TDI	Tapered roller bearing : two-row double-inner race configuration
UMP	Unbalanced Magnetic Pull
WT	Wind Turbine
WTDD	Land-based Wind turbine with direct-drive generator

1. Introduction

Direct-drive wind turbine generators are increasingly being considered as a commercially attractive option in the offshore wind industry [1]. Yet, their feasibility for floating offshore wind turbines remains to be established. So far, published reliability studies have shown that the aggregate failure intensities of drive-train in direct-drive WTs are greater than that of geared WTs [2]. These findings were based on electrically excited synchronous generators that use larger number of coils in larger diameter non-standardised machines , making them more prone to failure when exposed to arduous loading in the absence of gearbox [3].

Permanent magnet generators (PMGs) are likely to improve this situation. References [4-6], reported the structural design challenges in accommodating direct-drive generator for FWTs, but also pointed towards greater mechanical reliability as a potential incentive to redress the ensuing balance of costs. In principle, a direct-drive generator with fewer moving parts and half the number of components as that of the traditional geared system should present superior performance and greater mechanical reliability that is critical especially offshore [7]. Because of the low operational speeds, the generator is subjected to less wear, allowing a longer operational life and the capacity to handle larger operational loads.

Direct-drive generators are designed with stringent manufacturing tolerances and are particularly sensitive to dynamic changes in the air-gap that separates the rotor and stator. Possible consequences of these effects include imbalances in magnetic forces, vibrations, noise and bearing wear that can have an impact on the lifecycle of the drive-train components. Yet, there isn't enough operational experience from existing offshore wind turbines with direct-drive generators to corroborate this claim, designers are compelled to rely on numerical simulation techniques for making inferences on the dynamics of the drive-train [6]. Multi-body simulation (MBS) methods are widely used in the industry for this task. In this method, the various components in a wind turbine are modelled as rigid or elastic bodies connected by kinematic constraints or force elements and a set of computation algorithms solve the equations of motion. Such tools can provide expert insights into the dynamic loading of the drivetrain considering all relevant loading conditions and system-wide interactions that exist in a wind turbine system.

The first studies on the dynamics of a drive-train for FWTs were reported for a 750kW system by Xing *et al*., [8, 9]. The study employed MBS approach to de-couple gear behaviour

from turbine dynamics. The results showed greater shaft loading and internal drive-train responses (tooth contact forces, gear deflections and bearing loads) caused by wave and pitch induced motions of the FWT system. Their study also suggested greater fatigue loads and therefore greater cost implications for FWTs.

Few investigations on dynamics of direct-drive generator have been carried out in the past. References [10-12] analysed single-bearing radial flux direct-drive generator designs rated between 0.75-3MW levels. Experimental tests on a 1.5MW design showed no vibration problems with the generator, although up to 50% eccentricity was permitted during extreme loads. References [13, 14] quantified the excitations from cogging torque (a detent torque that is inherently generated by electromagnetic forces that depend on stator slot and magnet geometry) and torque ripple harmonics in the operational speed range of the turbine. Kirschneck *et al* [15] investigated the effect of magneto-mechanical coupling on the eigen behavior in a direct-drive generator.

The first studies with a direct-drive generator for a horizontal axis spar-buoy FWT system was carried out by Boulder wind power [16]. Their drive-train uses a modular light-weight air-core design of a 6MW axial flux permanent magnet generator with a flexible support structure. Preliminary results showed opportunities in nacelle weight reductions, reduction in extreme loads, savings in draft and tower structural requirements. With a low stiffness to weight ratio, the robustness of this generator system entirely relies on the effectiveness of stator-rotor air-gap control which can be difficult especially at higher magnitude nacelle accelerations. Reports on the drive-train behaviour are not yet available in public domain to make a detailed assessment.

Reference [6] took the first steps to understand the sensitivities of the direct-drive generator to air-gap dynamics, UMP and bearing loads by a fully coupled dynamic analysis using multi-body simulation tool, SIMPACK. The results showed a linear trend in eccentricity and UMP for a land based turbine. Considering the nature of loading in a FWT system, it is important to evaluate these sensitivities to verify the component design and durability.

This work aims to further this understanding by investigating the drive-train of a FWTDD system that was developed by the authors in a previous study [5]. To examine the drive-train dynamic behaviour, time-domain multi-body simulation tools namely HAWC2 [17] and SIMPACK [18] were used. HAWC2 is a multi-body simulation code that can simulate the time domain responses of a wind turbine by finite element modelling and coupling aero-hydro-servo-elastic behaviour. SIMPACK is also a multi-body simulation tool that allows detailed kinematic and dynamic analysis of wind turbine components by integrated wind turbine simulation, incorporating flexible Finite Element Methods (FEM) bodies, force and control elements. As the first step, the drive-train model proposed in [5] is implemented in SIMPACK and tested for land-based turbine model to quantify generator reaction in terms of eccentricity induced UMP and vibratory torque. The investigation then proceeds with a 2-step de-coupled approach for the FWT drive-train analysis. Such de-coupled analysis of drivetrain responses is applicable since the natural frequencies of the drivetrain vibrations are much higher than those of the natural modes of tower and blade vibrations or of rigid-body motions of a floating wind turbine, which are captured in the global response analysis. The global motion response and drive-train loads are obtained by 1-hour simulations in HAWC2 and then fed to a detailed stand-alone drive-train model in SIMPACK. The response statistics for shaft displacements, eccentricity, forces due to UMP, and the main bearing reactions were computed and compared with a land-based wind turbine model. The possible causes and

consequences of the nature of responses in a FWT are identified. The following sections describe the theory and methodology adopted for this study before proceeding with the discussions on drive-train modelling and analysis.

2. Theory and methodology

The de-coupled approach proposed by Xing *et al,*[9] is perfectly acceptable for geared drive-trains as the reaction forces are expected to be small. The gearbox response is of quasi-static nature with high frequency internal modes that are outside the region of wind turbine aerodynamic excitations. However, in the case of direct-drive generators the validity of this approach must be tested to obviate the significance of reaction forces. A preliminary investigation was carried out for a land-based wind turbine using SIMPACK considering a fully coupled system. This was intended to arrive at the drivetrain model that best characterised the dynamic behaviour of a direct-drive generator and served two purposes:

1) Internal drive-train reaction forces: To investigate the sensitivities of the drivetrain to shaft misalignment
2) Dynamic effects and Possible Feedback: To identify any unforeseen controller response action due to generator response

2.1 Internal drive-train response and feedback effects

In a FWT, the loads from the wind turbine coupled with the oscillatory motions at the nacelle can introduce high loads at the drive-train. The resulting interaction between assemblies in the drive–train may result in additional vibration or excessive forces. In a direct drive permanent magnet generator, the main reactions include (a) eccentricity induced unbalanced magnetic pull[19] and (b) shaft vibrations that manifest as bearing load and torsional vibrations in the drive-train[20].

2.1.1 Eccentricity induced unbalanced magnetic pull

The stator and rotor in a PMG are physically separated by a very small air-gap measuring a few millimetres. The non-uniformity of this air-gap (also termed as eccentricity) results in unbalanced magnetic pull (UMP) inside the machine. In a FWT, the probability of radial shaft misalignment is quite high which can be a major contributor to eccentricity. Shaft misalignment gives rise to a dynamically eccentric rotor disturbing the equilibrium of the magnetic attraction forces that result in a periodical radial load on the bearings, undesirable noise and vibration due to the increase in space harmonics [21]. Reference [4] introduced the analytical model to compute the UMP caused by eccentricity due to shaft displacement.

Fig.1 (a) shows a shaft-hub assembly displaced from the normal concentric arrangement. Fig. 1(b) shows a uniform distribution of the magnetic forces (shown by equal vector lengths) for a concentric rotor. Fig. 1(c) shows an eccentric rotor: as the shaft rotates and displaces from the centre as it rotates, the air gap distance is no longer spatially fixed but rotates with the rotor as well as the maximum and minimum force excitation, resulting in a dynamically asymmetric excitation of the generator. Intuitively, an unbalanced magnetic force results and it is pulling in the same direction of the displacement. This manifests as a net dynamic radial load on the bearings.

The net bearing load due to eccentricity was determined by using an approximate linear model that relates the percentage change in air-gap (i.e. eccentricity) to unbalanced magnetic forces [6, 21]. The generator model is of radial flux topology with interior rotor construction with permanent magnet pole pairs on rotor periphery and wounded copper coils on stator slots [22]. An air-gap measuring 6.36mm separates the rotor from the stator. The details of machine parameters are listed in Table 1.

With reference to Fig 1, the rotor is undergoing a counter-clockwise rotation along the x-axis and a translation in the positive Y-Z plane. Let $\delta y(t)$ and $\delta z(t)$ be the incremental shaft displacements, in the y-z plane, measured at any instant t. Then the dynamic change in air-gap, denoted as $g(t)$ can be obtained from the incremental shaft displacement along the Y and Z axis as

$$g(t) = \sqrt{\delta y^2(t) + \delta z^2(t)} \quad (1)$$

The ratio of this value to the nominal air gap, g_a is defined as the measure of dynamic eccentricity, *e(t)*

$$e(t) = \frac{g(t)}{g_a} \quad (2)$$

The unbalanced magnetic forces due to eccentricity were computed using magneto static simulations in Finite Element Methods Magnetics software (FEMM) [23]. Static eccentricity simulations were carried out as they represented the worst possible conditions that can be experienced by the rotor. The rotor was displaced from 3% up to 90% of the air gap length. The resultant force was obtained from the air gap flux density variation and was approximated as a function of the static rotor eccentricity ($e_{static} = g/g_a$) given by

$$F_{UMP\_STATIC} = 2291.8 \times e_{static} - 32.898 \ (kN) \quad (3)$$

The above expression for force represents the eccentric condition in steady-state (refer to Fig. 2). The magnetic stiffness of this system can be inferred from the slope of this curve. This model does not consider the effect of armature reaction on UMP as it is expected to be small [24]. A simple method for converting this force to represent dynamic eccentricity effects was done by accounting for the frequency of shaft displacements, ω_s. Together with dynamic eccentricity given by equation (2), the two different components of the resultant dynamic force along the y and z-axis were then resolved as

$$F_{YMAG}(t) = \{2291.8e(t) - 32.898\}\cos\omega_s t \ (kN) \quad (4)$$

$$F_{ZMAG}(t) = \{2291.8e(t) - 32.898\}\sin\omega_s t \ (kN) \quad (5)$$

The frequency of shaft displacements, ω_s can be determined from the knowledge of static deflection and the natural frequency of transverse vibrations. It must be remembered that the linear model assumption ignores the normal deflection of the generator structure and induced secondary deflection (as described in [25]). The bearing mechanical system acts as a spring-damper system with certain stiffness and damping. If K_Y and K_Z represent the radial components of bearing stiffness, the net restoring forces from the bearings is reduced by the magnetic stiffness of the system such that

$$F_{Y\_bearing}(t) = (K_Y - K_{YMAG})\delta y(t) \quad (kN) \quad (6)$$

$$F_{Z\_bearing}(t) = (K_Z - K_{ZMAG})\delta z(t) \quad (kN) \quad (7)$$

where magnetic stiffness components, K_{YMAG} and K_{ZMAG} are obtained by dividing equations (4) and (5) by the respective displacements. Typically the main shaft is modelled with 6 degrees of freedom, therefore axial and angular displacements also exist. While axial displacement does not disturb the magnetic equilibrium inside the generator, shaft tilting can contribute a UMP load which has a distribution depending on the air-gap distance [6]. The main bearings considered in the present study have large values of tilt component stiffness, therefore no effort was made to model the contributions to UMP as the tilt angles were expected to be less significant.

The equations (4) and (5) suggest that even at a non-eccentric condition there exists a residual force of 32.89 kN. This residual force appeared because of inaccuracies in modelling the slots and pole pairs in the FEMM model. For a given shaft displacement the force components due to UMP are assumed to act at the centre of the shaft where the rotor is attached (blue and red arrow lines in Fig. 3(a)) and tend to displace the shaft further in the

direction of original displacement. This implies that the forces act in a direction opposite to the restoring forces from the bearings (refer to Fig.3 (b)). As explained by the author in [4], for the air-gap to be stable, the radial stiffness of the bearings must be so chosen that the bearing reaction forces are greater than the UMP forces, i.e. $F_{radial\_bearing} >> F_{MAG(Y,Z)}(t)$. As with the linear model for UMP, the stiffness of the magnetic system is also assumed to exhibit linear characteristics.

2.1.2 Shaft displacement, vibratory torque and possible feedback effects

As the shaft of the wind turbine rotates, it is expected to undergo axial, transverse and bending displacement due to external loads. If the shaft is out of balance, displaced from the centre or if the shaft rotates at a speed equal to the natural frequency of transverse vibration, then the shaft begins to whirl, causing it to resonate. This can be very damaging to the wind turbine generator; especially the bearings and can also trigger pitch action if measurable reductions in torque occur. The most important natural modes of the drive-train must be examined with an emphasis to the influences of system parameters on the dynamics.

In the case of a rigid shaft, as the shaft is displaced away from the location of the centreline; the bearing stiffness constantly tries to restore the shaft back to the centre-line. Therefore the shaft orbits around the centreline as it rotates (the path shown by red dotted line in Fig. 3(b)). This can be imagined as a rotating mass that continually experiences a centrifugal force as it moves away from the centre of rotation(red arrow shows the direction of centrifugal force), and restored by inward pull from bearings(shown by blue arrow). If the displacement of the shaft is measured at every instant, *t*, then let the distance by which the shaft is displaced from the centre be *g*(*t*), given by equation(1). The centrifugal force on the rotor shaft assembly is given by [26]

$$F_{centrifugal} = m\omega_s{}^2(g(t)+s) \quad (8)$$

where, ω_s is the frequency of the shaft displacement, s is the static deflection. If m is the mass of the rotor shaft assembly, then the restoring forces from the bearings with stiffness, k must balance the centrifugal forces such that

$$m\omega_s{}^2(g(t)+s) = k \times g(t) \tag{9}$$

$$\omega_s = \omega_{nat}\sqrt{\frac{g(t)}{(g(t)+s)}} \tag{10}$$

where, ω_{nat} is the natural frequency of transverse vibrations $\left(\sqrt{\frac{k}{m}}\right)$. If the bearing stiffness is not high enough and the frequency of shaft displacement is high, it can reduce the available torque from the generator. The equation for available generator torque can be derived from first principles. Consider a mass with the rotational moment of inertia, I, rotating at an angular velocity, ω when a torque T is applied. Assuming the shaft also undergoes displacement from the centre, then in order that kinetic energy (E) is conserved during rotation

$$E = \frac{1}{2}I_1(\omega_1^2(t)) + \frac{1}{2}I_2(t)(\omega_2^2(t)) \tag{11}$$

where, I_1 the moment of inertia of the rotating mass, ω_1 is the angular velocity of the shaft. $I_2(t)$ is the moment of inertia of combined mass, m_2(shaft + rotor + turbine) displaced by a distance $g(t)$ from the centre, where, ω_2 is the frequency of shaft displacements(also denoted by ω_s). To compute the instantaneous torque, equation (11) is divided by time, t, and the intended frequency of rotation, ω

$$T(t) = \frac{1}{2\omega t}I_1(\omega_1^2(t)) + \frac{1}{2\omega t}I_2(t)(\omega_2^2(t)) \tag{12}$$

$$T(t) = T_1(t) + T_{vib}(t) \quad (13)$$

where T_1 is the available generator reaction after losses due to vibration T_{vib}.

3. Modelling generator response

To estimate the effect of shaft displacements on generator response, a fully integrated aerodynamic analysis was carried out on a land-based turbine (WTDD) in SIMPACK [6]. A detailed description of the turbine model is available in [6]; a simplified topology diagram of the drive-train system is shown in Fig. 4. The generator was assumed to be driven by the NREL 5MW baseline turbine [27]. The drive-line arrangement is similar to the commercial MTorres design described in [28] with the aerodynamic and gravitational loads supported by two main bearings housed on generator stator support structures. The bearing closer to the turbine rotor (BR2) is a double-row TDI bearing while the rear bearing (BR1) is a CRB, both represented as spring-damper elements. $J_{turbine}$, J_{shaft}, J_{rotor}, J_{stator} represent the moments of inertia of the respective elements. Two parallel load paths exist in a direct drive system and these are a combination of mechanical elements (turbine, main shaft, main bearings, generator structural support structures and bed-plate) and electromagnetic elements (generator stator/rotor magnetic circuits and air-gap). Torque is transmitted to the generator via the main shaft, while the main bearings transmit nontorque loads to the bed plate through generator support structure. As shown in Fig. 5, while transferring loads from/to the generator support structures, the main bearings complete the mechanical load path (1) while the air-gap between generator rotor and stator establishes an electromagnetic load path (2). The main shaft is a flexible beam element that supports the generator rotor with a 6DOF joint to account for the axial, bending and torsional loads. A force element between turbine and main shaft describes the torsional stiffness and damping of the rotor shaft as defined in [5]. The main shaft, generator stator, rotor, its housing and bedplate were modelled as rigid bodies, with

discretized stiffness and reduced degrees of freedom. The rotor blades were modelled as flexible bodies actuated by pitch control. Aerodynamic loads were generated using the AeroDyn interface in combination with Turbsim [29] using Kaimal turbulence model. The bearing elements, BR1 and BR2 were modelled using visco-elastic force element which allows the definition of full stiffness matrices provided by bearing manufacturer [30]. The bearings were modelled with C3 radial clearance values according to ISO-5753[31]. Sensors were used to measure the kinematic displacements of the rotor shaft and the rotor speed at every time step. The controller interface DISCON [27] enables a variable-speed, variable pitch operation according to 5 different control regions by measuring generator speed . The control laws for generator demand torque, $T_{Gen\text{-}i}$ (where i =1, 1-½, 2, 2-½, 3) were modified to suit the direct drive system (refer Table 2). The control algorithm accounts for pulsatory behaviour of the shaft (as defined in section 2.1.2) by computing the available torque at every time step, for the five control regions such that

$$T_{available}(t) = T_{Gen-i}(t) - T_{vib}(t) \tag{14}$$

DISCON also computes the eccentricity and UMP as defined by equations (4) and (5). These are used to establish the magnetic stiffness in the air-gap between rotor and stator (K_{MAG}). The results presented in [6] demonstrated that eccentricity increased linearly with wind speeds and UMP tends to follow the eccentricity profile.

The nature of drive-train response can be interpreted from its free and forced vibration characteristics. Table 3 presents the natural frequencies of the drive-train corresponding to the rigid body motions predicted by SIMPACK. It must be remembered that the bandwidth of external sources of excitation namely wind and wave loads lies between 0.021-12.5 rad/s and 0.376 -9.86 rad/s respectively[32], which are outside the excitation spectrum of the drive-train. The torsional mode is referred to the low speed shaft considering the main drivetrain

elements as rigid. A parametric study was carried out to examine the effect of different values of radial stiffness for the rolling element bearings on the frequencies of transverse vibration. It was assumed that the bearings do not undergo significant clearance change during steady-state operation, therefore the effect of changing clearances was not included in bearing load prediction. The equivalent radial stiffness of the two-bearing arrangement was 3.81E+10 N/m. Three cases were tested by decreasing the bearing stiffness in the radial direction from a base case by 20%, 25% and 30%. This resulted in up to 15 % reduction in natural frequencies (to 620.5 rad/s) which are well above the excitation frequencies of wind turbine loads thus precluding any opportunity for resonant behaviour. Thus the de-coupled analysis approach is valid for examining the internal responses in a direct-drive generator. This was further verified by examining the torque behaviour under normal operating conditions of the turbine.

A set of wind fields with mean wind speeds from 4-25m/s in accordance with the normal turbulence model as per IEC 61400 [33] were used for generating the blade aerodynamic loads. Twenty-two one hour simulations were carried out and time histories of vibratory torque and blade pitch angle (β) were monitored. Fig. 6 shows a comparison of time histories of the vibration induced torque measured for two cases 4m/s and 12m/s. It was observed that the torque fluctuations generally increased with increase in wind speeds.

To validate the torque behaviour, comparison was made to another land-based system (WTDD) created in HAWC2 [5]. This model also uses the NREL's 5MW turbine for simulating the aero-elastic response but the wind field uses Mann turbulence model. Reference [5] provides a detailed description of the model; for the purpose of brevity, only the block diagram of drive-train is shown in Fig. 4(b). The drive-train had an ideal pitch control and torque behaviour defined by a 1-DOF torsional spring damper system. Fig. 4(b)

shows a simplistic lumped 2-mass representation of the turbine and the generator with the main shaft modelled as a Timoshenko beam element supported by two bearings defined using constraint equations. A quasi-static response was assumed from the generator; the electromechanical response of the generator including UMP and torque loss was not modelled, so the controller interface DISCON (a dynamic link library) only serves to demand torque from the generator $T_{Gen\text{-}i}$ and control the blade pitch angle. The HAWC2 model was also tested in 22 similar wind conditions; the torque and blade pitch angle time histories for one-hour simulations were extracted. A comparison of the results with SIMPACK simulations was performed to detect any spurious pitch action due to the generator. The difference in the response, Δ was computed and expressed in percentage using

$$\Delta = \frac{X_{SIMPACK} - X_{HAWC2}}{X_{HAWC2}} \times 100 \quad (15)$$

where, $X_{SIMPACK}$ is the response variable measured from the SIMPACK simulations and X_{HAWC2} is the corresponding value from the HAWC2 model. Fig. 7 shows the percentage difference in mean values of torque and blade pitch angles estimated from both tools. As may be noted, no pitch action was predicted by both the models until about 10m/s of wind speed. At higher wind speeds a maximum of 15% difference existed between the two models. The mean values of torque obtained from both the models were quite similar although SIMPACK model accounted for some losses due to vibration (for example, at 12m/s wind speed, $T_{\text{mean\_HAWC2}}$= 4.82MN-m and $T_{\text{mean\_SIMPACK}}$=4.76MN-m). Fig. 8 shows the vibratory torque expressed as a percentage of operating torque. The mean, standard deviation and maximum values remained below 0.5% of the operating torque.

It is recognized that mechanical vibration can also be excited by cogging torque, or any structural flexibilities that can introduce additional forces and vibrations due to whirling. However, no effort was made to examine these effects, although some studies suggest the

permissible limit of vibratory torque due to cogging is of the order of 1.5-2% of rated torque [13]. Since the variation due to shaft eccentricity is limited to below 0.5% of rated torque, it is expected that the efficiency of power transfer will not be affected. With the torque and blade pitch angles from both systems being similar for the range of wind speeds studied, it is reasonable to assume that the shaft displacements occurring during normal operation are not large enough to reduce the available mechanical torque or alter the blade pitch action. Thus, these results show that it is reasonable to ignore the feedback effects and spurious pitch trigger action in a direct-drive generator.

4. Analysis of FWTDD drive-train system using the 2-step de-coupled approach

As mentioned in section 2, the two-step decoupled approach is adopted. This approach is explained in great detail by Xing *et al.*, [9]. Hence only a brief description is provided here. As a first step, fully coupled aero-hydro-servo-elastic simulations for the FWTDD system were carried out in HAWC2. The time histories for global motion response and main shaft loads from HAWC2 simulations were input to a detailed drive-train model in SIMPACK. The internal responses and loading of the drive-train were analysed in SIMPACK.

4.1. HAWC2 model of the FWTDD system

The floating version of the direct drive wind turbine was built in HAWC2 for the specifications presented in [5]. The mooring lines use a simplified spring model describing the force-displacement relationship but neglecting the effects of damping and inertia. The main specifications for the turbine and drive-train are listed in Table 4. HAWC2 computes the loads on various components of the wind turbine, solves the equations of motion by a time integration scheme and presents the results as time series of forces, moments, and deformations. 6DOF motion sensors provide the instantaneous nacelle position, velocity, and

accelerations while sensors for the drivetrain provide the main shaft moments and forces. These will feed into a stand-alone SIMPACK model.

4.1.1 Design Load Cases

This study was aimed at making initial empirical inferences on the dynamics of the direct-drive system. Hence, to begin with, the consistency and performance of the drive-train was verified for normal power production. In order to consider representative environmental conditions with turbulent wind field and irregular waves, long-term joint wind and wave data were correlated for a representative site (Statfjord in North Sea) from site measurements using the analytical models that relate the expected values of significant wave height $E(H_{m0})$ and peak wave periods $E(T_P)$ to a 10-min mean wind speed at hub height, V[34]. The long-crested irregular waves were represented by Joint North Sea Wave Project (JONSWAP) spectrum and turbulence intensity for class "C" was applied for the wind fields. The typical operating region of the wind turbine covered the mean wind speeds from 4-25m/s with corresponding significant wave heights between 1.96-5.88m. The correlations are presented in [5].

4.2. Stand-alone SIMPACK models for the WTDD and FWTDD generator

The output from the shaft and nacelle position sensors from HAWC2 simulations are basically time series which feed-in to a stand-alone drive-train model in SIMPACK (Fig. 9). The drive-line arrangement for the FWTDD system is similar to the WTDD system as described in section 3 comprising the main shaft, two main bearings and the generator. In SIMPACK, both the systems were modelled with the mass and inertia representing the nacelle and the drive-train segregated from the turbine, blade pitch actuator, hub and tower. For the FWTDD system, the platform and mooring sections were also excluded (Fig. 10 shows the topology diagram). Thus the main elements considered in the de-coupled dynamic

analysis include the main shaft, main bearings and the generator. The dynamics from the rest of the drive-train including power electronics and conversion equipment were excluded from the analysis. For the WTDD system, these were lumped as passive elements contributing to the mass and inertia at the nacelle. In the case of the FWTDD system, these elements were relocated to the tower bottom [5] hence the nacelle of the FWTDD was lighter than the WTDD system. The tower and platform action were replicated by a dummy body steered by a 6DOF joint that accepts the position, velocity and acceleration inputs from the respective HAWC2 models. The shaft moments, forces and torque input from HAWC2 are applied as time excitations by using force element FE-93. The two components of the UMP (Y and Z) computed at each instant from the shaft displacements and applied between stator and rotor using force element FE-50. The generator reaction torque is modelled using force element FE-110, a proportional actuator which applies the generator torque determined by using the shaft speed from the HAWC2 simulations as the reference input(ω_{ref}) as

$$T = K_p(\omega - \omega_{ref}) + K_I \int_0^t (\omega - \omega_{ref})dt \quad (16)$$

where, $(\omega - \omega_{ref})$ and $\int_0^t (\omega - \omega_{ref})dt$ are the speed error and the integral speed error respectively. K_P and K_I are the proportional and integral gains for the controller. The proportional gain of the controller was chosen to be the slope of region 2 of the respective torque-speed characteristics [5,6]. The integral gain was chosen to minimise the steady-state speed error to less than 0.5 rad/s. The stand-alone drive-train models for the WTDD and FWTDD systems were tested with the respective loads extracted from the 22 load case simulations from HAWC2 and the internal responses were quantified.

5. Drive-train responses from global response simulation

Reference [5] reported the HAWC2 results from 22 one-hour simulations for the WTDD and FWTDD systems. The time series of main shaft loads were extracted to enable further analysis and comparison of the response statistics. A marginal increase was observed in the mean, standard deviation and maximum values of torque, axial forces, shear forces and bending moments for the FWTDD system. The mean bending moments and shear forces predicted by HAWC2 were smaller for FWTDD below rated wind speeds. Further, the load spectra suggested that the impact of wave excitation and platform's pitch natural frequency could be felt by the load bearing components (e.g.: bearings) in the drivetrain for the FWTDD system. With this knowledge, the following section explores the internal drive-train behaviour in detail.

6. Internal drive-train response in SIMPACK

A set of response variables was used as a measure of the reaction of the drive-train to the combined loading from wind and nacelle accelerations observed in the WTDD and FWTDD systems. These include shaft displacements and forces due to UMP and the load components on the main bearings (axial, radial loads and tilting moments). These were treated as primary response variables. There can be other reaction forces and induced secondary responses that can be expected as a result of the main shaft loads and the primary responses. For example, the shaft can undergo structural deflection and generator structural members can also deflect due to UMP. However no effort was made in this paper to study these responses or the effect of these on the main response variables.

In the following, a comparison of the primary response variables for the FWTDD and WTDD systems is presented. Figures 11-13 show the percentage differences in the mean, standard deviations and maximum values of forces due to UMP, bearing forces and tilting moments of

BR1 and BR2, radial and axial shaft displacements of the FWTDD system in comparison with the WTDD system. These were computed using [5]

$$\partial = \frac{\left(X_{FWTDD} - X_{WTDD}\right)}{X_{WTDD}} \times 100 \quad (17)$$

where, X_{WTDD} is the response variable measured from the land based model and X_{FWTDD} is the corresponding value for the offshore floating model. The results for axial response variables overlap with each other and are hence plotted separately. The results of main shaft loads predicted by HAWC2 are interleaved to understand correlation between global responses and detailed drive-train reaction. HAWC2 predicts less than 6% difference in the mean values of main shaft loads; this would result in up to 10% difference in response variables as predicted by SIMPACK. While HAWC2 predicts less than 1% increase in shear forces with the FWTDD system, SIMPACK predicts a measurable increase in radial response variables with wind speed (viz., radial shaft displacements and UMP). Similar trend can be observed for the bearing moments. The increase in mean, standard deviation and maximum values of axial response variables generally follow the trend predicted for shaft axial forces by HAWC2 simulations. The quantum of increase predicted for the FWTDD system is much smaller than HAWC2 predictions, yet it is reasonable to conclude that the axial response of the direct-drive system varies linearly with shaft axial forces. The standard deviation in radial responses is significantly smaller than shear forces predicted by HAWC2. The maximum values of radial response variables tend to oscillate with up to 22% difference (for e.g.: in bearing BR2 tilting moment) observed from SIMPACK and 15% difference (for e.g.: in main shaft bending moments) predicted by HAWC2. In summary, the comparison demonstrates the importance of higher fidelity drive-train models in accurately characterizing the dynamic response. The likely causes and consequences of the drive-train response characteristics (Figs. 11-13) are discussed in detail in the following sub-sections.

6.1 Shaft Displacements

For a direct drive generator, proper shaft alignment and hence the concentricity is greatly influenced by the nature of shaft loading, the durability of bearings that support the shaft rotor assembly and the degree of compliance. The bearing stiffness sensitivity study discussed under section 3 was extended to examine shaft radial displacements and forces due to UMP. The case with 20% lower stiffness was chosen as it still resulted in tolerable operating conditions without considerably changing the air-gap eccentricity, UMP and the bearing loads [4]. The steady state deflection for the chosen level of compliance resulted in 0.3% eccentricity and the mean dynamic air-gap eccentricity was about 10%. As explained under section 2.1, shaft displacements are possible along 6DOF, when treated separately, only few components are expected to disturb the magnetic equilibrium inside the generator. Fig. 14 shows the main types of displacements and their possible effects on UMP.

6.1.1 Eccentricity and UMP

Eccentricity was computed from the instantaneous shaft displacements in the radial direction normalized to the nominal air gap of concentric rotor (equation (2)). Fig.15 shows the plots for the mean and maximum % eccentricity observed for both the systems for the different wind speeds. With increase in wind speeds, the mean values for radial shaft displacements were observed to linearly increase from 0.19mm at 4m/s to 0.66mm at 25m/s which resulted in 10.4% eccentricity at 25m/s for the WTDD system. The allowable air-gap deflection for the direct-drive system is generally within 10–20% otherwise the airgap flux density will increase significantly [35]. The FWTDD system led to very small increase in these values (2.2% at an average) which are still within the design tolerance. The maximum difference in mean values of radial displacements for the FWTDD system was still low (i.e. 6%) and occurs at a wind speed of 25m/s. The percentage difference in standard deviation values for

radial displacements between the two systems also followed the same trend as the mean values. The maximum value of shaft displacement can reach up to 2.2mm (i.e. about 36% eccentricity) for the WTDD system at 25m/s wind speed. Since this is a momentary phenomenon, it is expected that this will not introduce secondary deflection. With the FWTDD system, the relative change in maximum values lies within ± 10%, with greatest difference at 6m/s. The results also suggest that no possible air-gap closure occurs with the FWTDD system even with lower bearing compliance for the range of wind speeds studied. The comparison of power spectra (Fig. 16(a)) for the two systems show very negligible difference in the energy content implying no additional excitations from platform motions or wave frequencies. It may be noted that the highest frequency considered in these plots is about 20 rad/s, which is smaller than the lowest natural frequency of the drivetrain (of the torsional mode), Since the main excitation frequencies remained within this region, the analyses were limited to this bandwidth.

The net UMP forces can be resolved using the eccentricity measurements in the Y and Z directions. Since UMP forces have a linear relationship with eccentricity, the trend observed in Fig. 15 is expected to be preserved in the case of UMP forces as well. It is therefore reasonable to infer that FWTDD system is not subjected to additional sporadic excitations that are either wave/motion induced.

6.1.2 Axial Shaft displacement

The main bearings supporting the shaft for WTDD system were generally calibrated to accommodate large thrust loads so that the axial shaft displacement(runout) and the movement of the generator rotor with respect to the stator is relatively very small. The FWTDD system noticeably experiences an increase in the axial loads and hence greater axial displacements. The trends in the axial displacements (% difference in mean values and

standard deviation) matches with that of the main shaft axial forces predicted by HAWC2. The maximum difference in mean values (about 10%) appears for a wind speed of 12m/s. With the absolute values of standard deviations being small a slightly larger percentage difference (40% at 4m/s) was observed with the main shaft axial displacements in the FWTDD system. The maximum values for shaft displacements increase by about 17% at an average for the FWTDD system, with the greatest difference (25%) observed at 23m/s. As may be noted from the power spectra (Fig.16 (b)), this difference is induced by platform pitch motions and wave excitation. If L is the axial length of the rotor, for a shaft displacement measuring dx mm, the rotor also displaces by dx mm with respect to the stator(Fig. 14(c)). Since both the generator rotor and stator structures are symmetric along the axial direction and no skewing of rotor magnets was assumed to exist, axial displacement by itself is not expected disturb the magnetic equilibrium inside the generator . Since eccentricity is constant down the axial rotor length, only the portion L-dx of the rotor will be effectively involved in UMP. With regards to the generator response, if tilt displacements are small, then larger axial run-out in FWTDD system is not expected to alter the electromagnetic forces , however greater wear from sliding can be expected in bearing rollers [36].

6.1.3 Main Shift Tilt displacements

Shaft tilting causes the shaft-rotor assembly to be not parallel with respect to the stator, since this results in a non-uniform eccentricity along the axial length of the rotor, changes of the magnetic field in the axial direction may have to be included in the UMP model using 3-dimensional analytical solution. The distribution depends on the air-gap distance (maximum load in the region with lowest air-gap and vice-versa) [6]. Since the TRB tilt stiffness in the studied model was calibrated to be sufficiently high, the shaft did not undergo considerable tilting, therefore three-dimensional effect was not included in the UMP model. The pitch and

yaw angles (θ_y and θ_z) observed for a wind speed of 20m/s were considerably small as may be noted from the time histories in Fig. 17. The frequency spectra in Fig. 16(c) & 16(d) shows turbine 1P excitation as the most dominant frequency, no additional excitations in the FWTDD system are observed that are neither motion induced/wave induced .

6.1.4 Bearing Loads

In general, the bearing stiffness characteristics determine the reaction at the bearings. As with the WTDD system, BR2 was tuned to accommodate the majority of thrust loads and hence the axial reactions from bearing BR2 are greater than BR1 by a factor of approximately 7.5. The bearing axial loads for the FWTDD system are correlated to the wind turbine thrust force which has a decreasing mean value for wind speeds larger than rated (i.e. 12m/s) due to pitch control[6]. As may be noted from Fig. 18, BR2 in the FWTDD system experiences an increase in axial load with the maximum and mean values reaching up to 1380kN and 775kN at 12m/s. The increase in standard deviation and maximum values (Fig. 12(b) and 13(b)) for the bearing axial loads for the FWTDD system are yet again attributed excitations due to wave and platform pitch motions. The shape of the power spectra for the bearing axial loads (BR2) and axial displacements are similar (Figs 16(b&e)), so the linear relationship is preserved in the FWTDD system.

For the WTDD system, it was observed that the radial loads in bearing BR2 are greater than BR1 by a factor of at least 2 until 20m/s wind speed. At greater wind speeds, the reactions tend to be comparable. For the WTDD system, the mean values of radial loads vary linearly with increase in wind speeds (Fig. 19). The mechanics on the FWTDD system differ by less than 10% and 15% respectively for the mean and maximum values. Despite acting like a negative spring that abates the restoring from bearings, the forces due to UMP contributes to

less than 3% reduction in the overall mechanical stiffness. Fig. 20 compares the time histories for UMP and radial bearing load (BR2) at 25m/s wind speed. If secondary deflections can be assumed to be small, the presence of UMP does not necessarily bring about a perceptible increase in bearing reactions. This was attributed to the large value of the bearing to magnetic stiffness ratio ($k_{bearings}/k_{mag}$) at all the wind speeds. The mean values of tilting moments for BR2, being a TRB tend to increase linearly for the WTDD system. The FWTDD system introduces an average increase of about 7% in the mean and standard deviations. The differences in maximum values are as high as 22% (16-17m/s). The comparison of frequency spectra for the two systems (Fig. 16(f)) shows additional energy content for BR2 around the wave frequency and platform pitch frequencies. BR1, being a CRB undergoes substantially lower tilting with less than 4kNm at 25m/s wind speed, hence the results are not discussed. It may be observed that the mean bending moments and shear forces predicted by HAWC2 are smaller for FWTDD below rated wind speeds (Fig. 11-13). However, at these load levels, the actual values of mean bearing moments and radial forces predicted by SIMPACK are higher in FWTDD system and hence this results in a positive difference. Since the radial shaft displacements in FWTDD system are larger than WTDD this generates additional forces due to UMP which has to be reacted by the bearings. Overall, a subtle shift exists in loading behavior of bearings for the FWTDD system as compared to the WTDD system. Further studies examining fatigue damage can help verify their durability.

7. Conclusions

The work presented in this paper extended the investigations on a direct-drive radial flux permanent magnet generator model that was custom built for a floating spar buoy type wind turbine. Preliminary investigations on a multi-body WTDD system were used to understand and model the electro-mechanical reaction at the generator. Two load paths were identified

for the direct-drive PM system: mechanical load path realised by main bearings that transfer loads from/to the generator support structures and electromagnetic load path formed by air gap that transfers the electromagnetic forces to the generator support. The forces due to UMP act as a negative linear spring that tends to weaken the restoring force from bearings. It was observed that the feedback forces from the generator were not large enough to propagate to the turbine or initiate pitch action and can be small enough to be ignored. The main reactions from the drive-train including eccentricity, UMP and frequency response are sensitive to bearing compliance.The internal dynamics of the drive-train was analysed under normal operation using a combination of a fully coupled aero-hydro-servo-elastic model of the FWTDD system in HAWC2 and a detailed drive-train model in SIMPACK. The global motion response and main shaft loads from HAWC2 simulations were fed to a discrete 6-DOF drive-train model in SIMPACK to examine the component loading and response behaviour. The response variables studied include shaft displacements, forces due to UMP and the main bearing loads. A comparison with land-based system was useful in making the following inferences:

- Drive-train model: The axial response variables of FWTDD drivetrain demonstrated a more or less linear behaviour with regard to the main shaft axial loads predicted by the HAWC2 model. The dynamic content of radial and tilt components of response variables predicted by SIMPACK emphasise the importance of higher model fidelity is representation of drive-train dynamics.
- Shaft displacements & eccentricity: Upto 25% increase was observed for maximum axial displacements in the case of FWTDD system, these were mostly induced by wave excitations and platform pitch motions. Also, no significant shaft tilting was observed owing to a high bearing tilting stiffness. Owing to the symmetrical nature of the generator

structure and no skew effects considered, the axial displacements are not expected to affect the nature of electromagnetic response of the generator; however this implies a greater sliding in rollers of the bearings increasing the risk of failure from wear. Radial displacements (hence eccentricity) tend to increase linearly with wind speeds. FWTDD system does not bring about any significant increases to these values with the mean values limited within the generator design tolerances. Also the possibility of air-gap closure did not arise.

- Forces due to UMP: The forces due to UMP were modelled to have a linear relationship with eccentricity. Since eccentricity varies linearly with wind speeds, it is reasonable to infer a similar trend for the forces due to UMP. Also, since no additional excitations were observed in the eccentricity measurements, the FWTDD system is not expected to not increase these forces considerably.
- Bearing loads: Upto 22% increase in bearing axial loads was observed for the FWTDD system. The forces due to UMP, despite acting as a negative spring do not escalate the bearing radial loads. This was possible because of a large value of stiffness ratio ($K_{bearings}/K_{mag}$). The larger standard deviations in rotor end bearing axial loading and tilting moments were caused by wave frequencies and platform motions. Further studies examining fatigue damage can help verify their durability.

Further research including the secondary responses (e.g.: generator structural deflection due to UMP) can provide more insight on detailed dynamic behaviour. It is anticipated that the extra investment on the structural requirements for the FWTDD system will be outweighed by superior reliability with the direct-drive generator. Additional load cases including transient events encompassing grid dynamics can help verify this hypothesis.

Acknowledgments

This work was carried out at as part of the MARINA Platform project, Grant Agreement no 241402, funded by the EC Seventh framework programme theme FP7 ENERGY in Collaboration with the faculty of Engineering Science and Technology, Norwegian University of Science and Technology (NTNU), Trondheim Norway. The authors would like to thank Kaswar Mostafa (University of Edinburgh) for his inputs on eccentricity models.

References

[1] A. M. Ragheb and M. Ragheb, Wind Turbine Gearbox Technologies.Available at http://cdn.intechopen.com/pdfs/16248/InTech-Wind_turbine_gearbox_technologies.pdf. [Accessed, September 2015].

[2] H. Arabian-Hoseynabadi, P. J. Tavner, H. Oraee, Reliability comparison of direct-drive and geared drive wind turbine concepts. Wind Energy 2010; 13:62–73, DOI: 10.1002/we.357

[3] M.W.G.Whittle, Wind Turbine Generator Reliability: An Exploration of the Root Causes of Generator Bearing Failures,PhD Thesis,Durham University,2013.

[4] L. Sethuraman, V.Venugopal, A. Zavvos, M. Mueller, Structural Integrity of a direct-drive generator for a floating wind turbine. Renewable Energy. Volume 63, March 2014, 597–616.

[5] L. Sethuraman, Y.Xing, V.Venugopal, Z. Gao, M.A. Mueller, T. Moan. A 5MW direct-drive generator for floating spar-buoy wind turbine : Development of a fully-coupled Mechanical model .Proceedings of IMechE: Part-A Journal of Power and Energy, June 2014, doi:10.1177/0957650914537262.

[6] L. Sethuraman, Y. Xing, Z.Gao, V. Venugopal, M. Mueller, T. Moan. A multi-body model of a direct drive generator for a wind Turbine. In the Proc. of EWEA 2014, 10 March - 13 March, Spain.

[7] Haliade 150-6MW Offshore wind turbine, Available from: http://www.alstom.com/Global/Power/Resources/Documents/Brochures/offshore-wind-turbine-6mw-robust-simple-efficient.pdf, Accessed September 2015.

[8] Y.Xing, M.Karimirad and T. Moan. “Effect of Spar-Type Floating Wind Turbine Nacelle Motion on Drivetrain Dynamics”. In the Proc. of EWEA 2012 Annual Event, Copenhagen, Denmark, 16-19 April 2012.

[9] Y. Xing, M. Karimirad, T. Moan. Modelling and analysis of floating spar-type wind turbine drivetrain. Wind Energy. February 2013. DOI: 10.1002/we.1590.

[10] R. Poore and T. Lettenmaier.Alternative Design Study Report: WindPACT Advanced Wind Turbine Drivetrain Designs Study.2002.

[11] G. Bywaters, V. John, J. Lynch, P. Mattila, G. Norton, and J. Stowell, M. Salata, O. Labath, A. Chertok and D. Hablanian. Northern Power Systems-WindPACT Drivetrain Alternative Design Study Report. April 12, 2001 to January 31, 2005.

[12] G. Bywaters, P. Mattila, D. Costin, J. Stowell, V. John, S. Hoskins, J. Lynch, T. Cole, A. Cate, C. Badger, and B. Freeman . Northern Power NW 1500 Direct-Drive Generator . NREL/SR-500-40177 October 2007

[13] J. V. Ruuskanen,J. Nerg, J. Pyrhonen. Dynamic Torque Analysis of a Wind Turbine Drivetrain Including a Direct-Driven Permanent-Magnet Generator. IEEE Transactions on Industrial Electronics,Vol:58 , Issue: 9 , Sept. 2011.

[14] J. Heikkinen, J. Sopanen, V. Ruuskanen, and J. Nerg, Dynamic analysis of a direct-driven permanent magnet generator drivetrain including flexible turbine blades, in Proc. of the ASME International Design Engineering Technical Conferences Computers and Information in Engineering Conference, IDETC/CIE 2011, Washington, DC, USA, Aug. 2011.

[15] M. Kirschneck, D. J. Rixen, H. Polinder, Ron A.J. van Ostayen, Electro-Magneto-Mechanical Coupled Vibration Analysis of a Direct-Drive Off-Shore Wind Turbine Generator, ASME. Journal of Computational and Nonlinear Dynamics.. 2015;10(4):. doi:10.1115/1.4027837.

[16] Boulder Wind Power. Advanced Gearless drivetrain-Phase I Technical report .U.S. DOE Wind and Water Power Program. August 2012.

[17] T.J. Larsen and A.M. Hansen, How 2 HAWC2, the user's manual Risø National Laboratory, Technical University of Denmark, Lyngby, Denmark 2012.

[18] SIMPACK.Welcome to SIMPACK, http://www.simpack.com/.[Accessed, September 2015].

[19] Y.K. Chin, P. Kanninen, P. Maki-Ontto, R. Sakki, H. Lendenmann, Phenomenon of Magnetic Force in Permanent Magnet Wind Turbine Generators, International Conference on Electrical Machines and Systems, 2009. ICEMS 2009. 15-18 Nov. 2009, Tokyo

[20] M.Whittle, W. Shin, J.Trevelyan, J.Wu. A Parametric Study of the Effect of Generator Misalignment on Bearing Fatigue Life in Wind Turbines, in Proc. of EWEA 2011, Brussels.

[21] K. Mostafa, L. Sethuraman, M. Mueller, Unbalanced Magnetic Pull Comparison of Air-gap Winding and Iron-cored Permanent Magnet Machines for Direct Drive Wind Turbine. In the Proc. of EWEA 2014, 10 March - 13 March, Spain.

[22] D. Bang, Design of Transverse Flux Permanent Magnet Machines for Large Direct-Drive Wind Turbines. PhD Thesis, Delft University of Technology, Delft, The Netherlands, 2010.

[23] D. Meeker, Finite Element Method Magnetics Version 4.2 User's Manual October 16, 2010.

[24] J.Shek, D.G. Dorrell, M. Hsieh, I-Hsien Lin, K. Mostafa, M.A. Mueller, Yu-Han Yeh,Unbalanced forces in electrical generators for wave and tidal devices,10th European wave and tidal energy Conference,Aalborg, Denmark,2-5 September 2013.

[25] A. S. McDonald, Structural analysis of low speed, high torque electrical generators for direct drive renewable energy converters, PhD Thesis, The University of Edinburgh, 2008.

[26] S. Dunkerley. On the Whirling and Vibration of Shaft. Philosophical Transactions of the Royal Society of London. A , Vol. 185, (1894), pp. 279-360.

[27] J. Jonkman, S. Butterfield, W. Musial, G. Scott, Definition of a 5-MW Reference Wind Turbine for Offshore System Development. NREL/TP-500-38060, February 2009.

[28] J.N.Stander, G.Venter,M.J. Kamper, Review of direct-drive radial flux wind turbine generator mechanical design. Wind Energy, 2012;15:459-472. DOI: 10.1002/we.484

[29] N. Kelly, J. Jonkman, NWTC Design Codes (TurbSim),Available from: http://wind.nrel.gov/ designcodes/preprocessors/turbsim/, Accessed:September 2015.

[30] TIMKEN Linearised bearing stiffness Calculation. E-mail Communication. January 2013.

[31] ISO 5753:2009, Rolling bearings -- Internal clearance -- Part 1: Radial internal clearance for radial bearings.

[32] Vannuci(RINA Industry), D., ORECCA.WP3 Technologies state of the Art,Available from: http://www.orecca.eu/c/document_library/get_file?uuid=144f87d6-c41a-4a04-8742-7ebdc88f5a5c&groupId=10129, Accessed:September 2015.

[33] IEC 61400-1: Design Requirements for Offshore Wind Turbines, 1st edn, 2009.

[34] M.Karimirad and T. Moan, Wave and wind induced dynamic response of a spar-type offshore wind turbine. Journal of Waterway, Port, Coastal and Ocean Engineering 2012. 138(1): p. 9-20.

[35] A.S. McDonald, M.A. Mueller, H. Polinder, Structural mass in direct-drive permanent magnet electrical generators, IET Renewable Power Generation. 2007, doi: 10.1049/iet-rpg:20070071.

[36] L.Sethuraman, Y.Guo,S. Sheng, Main bearing dynamics in three-point suspension drive-trains, presented at AWEA windpower conference, 18-21 May 2015, Florida.

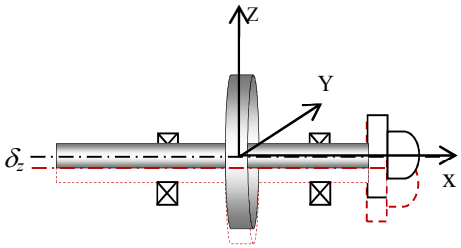

Fig. 1 (a) Shaft Displacement

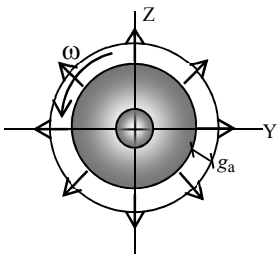

Fig.1(b) Concentric Rotor

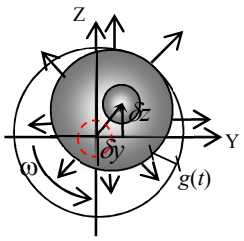

Fig.1(c) Eccentric Rotor

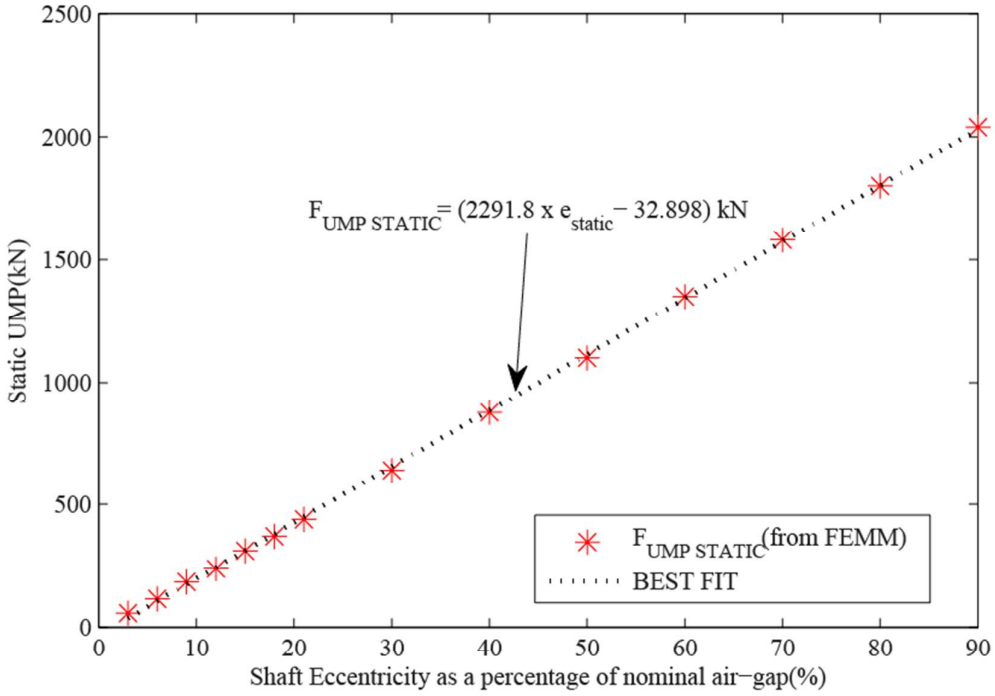

Fig. 2 Eccentricity Vs Forces due to UMP

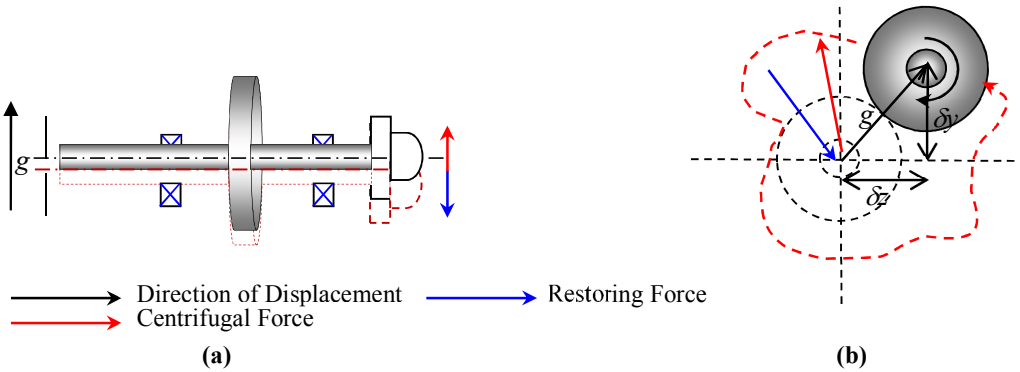

Fig. 3 Shaft behaviour (a) Shaft displaced from centre (b) Shaft Orbital motion

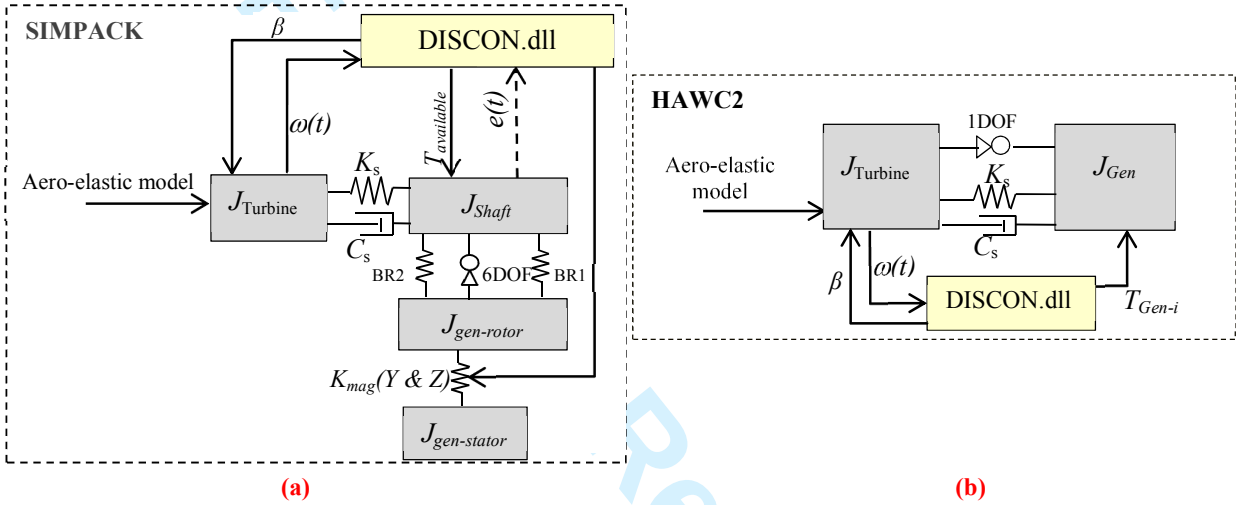

Fig. 4 Basic block diagrams for drive-train models (a) SIMPACK (b) HAWC2

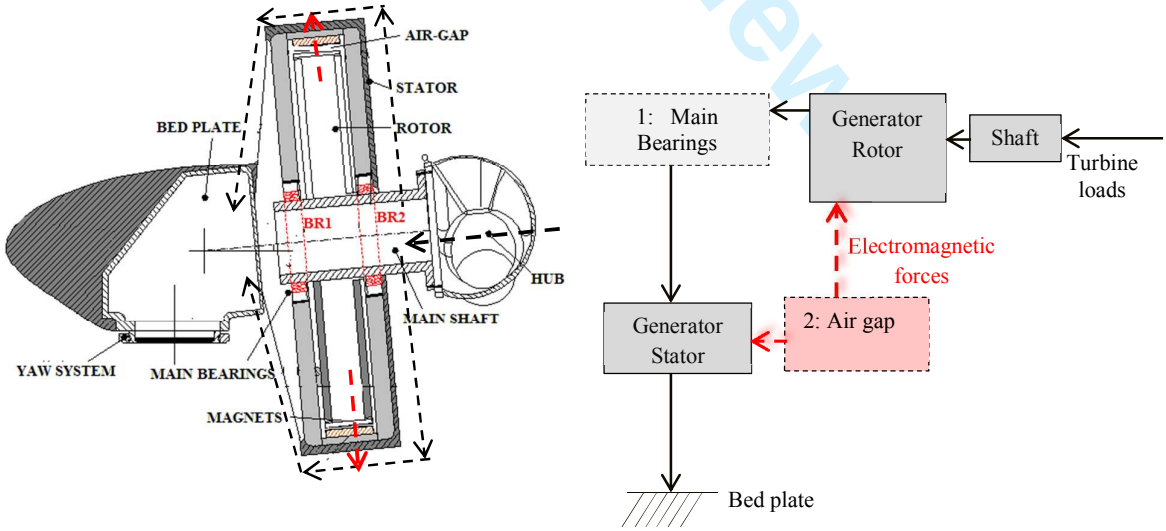

Fig. 5 Load paths in the studied direct-drive generator

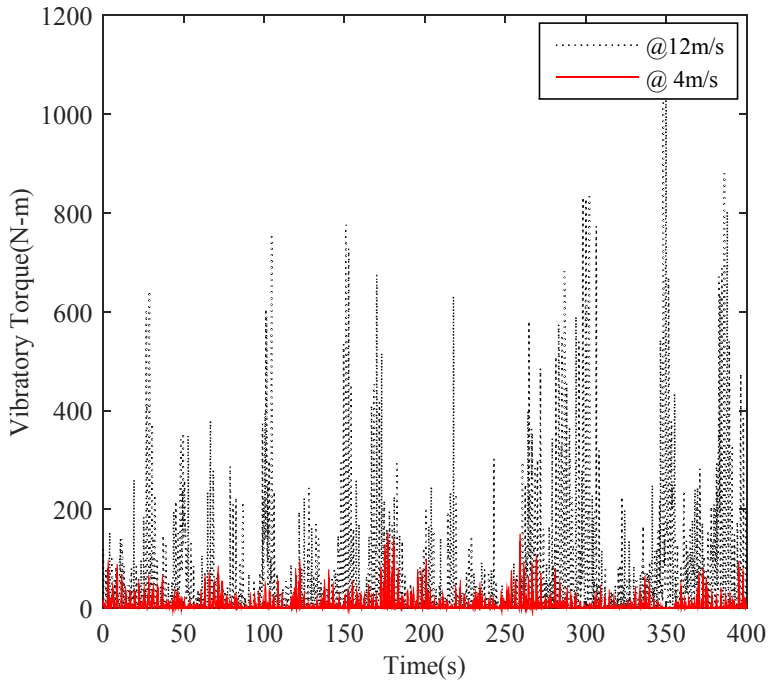

Fig. 6 Time history of Vibratory torque measured by SIMPACK

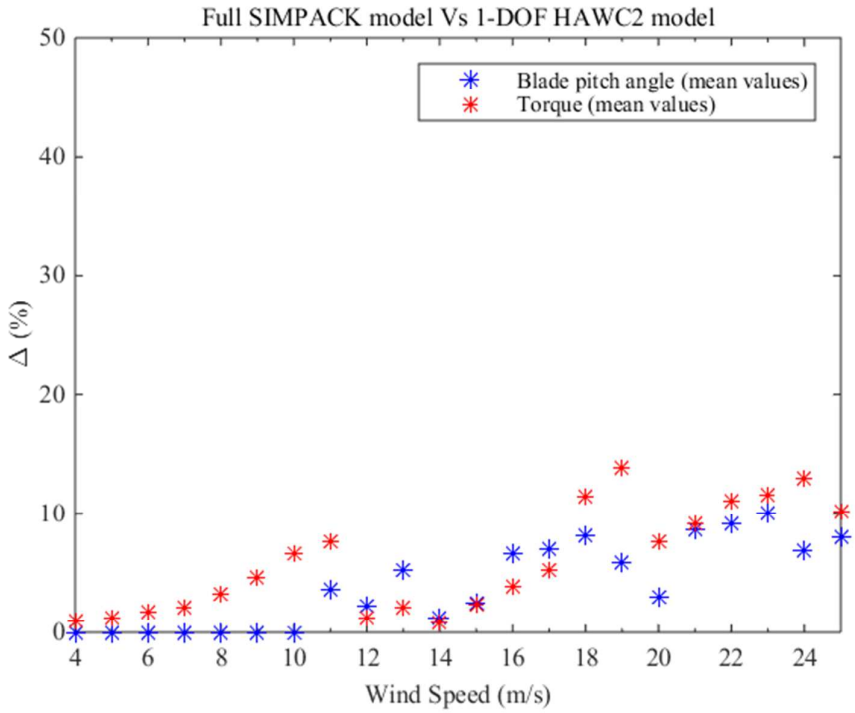

Fig. 7 Blade pitch angle response and generator torque for different wind speeds

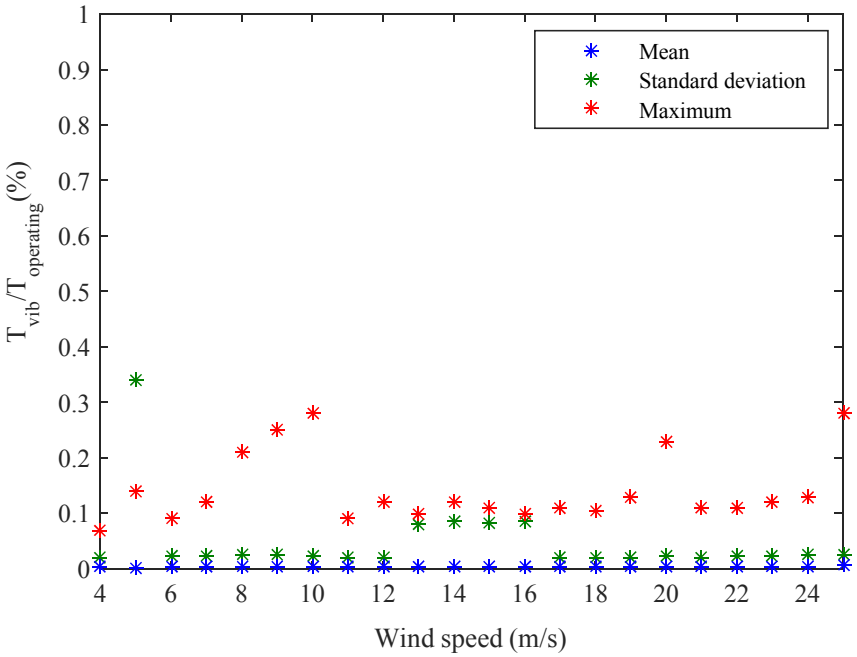

Fig. 8 Vibratory Torque as a percentage of Operating Torque

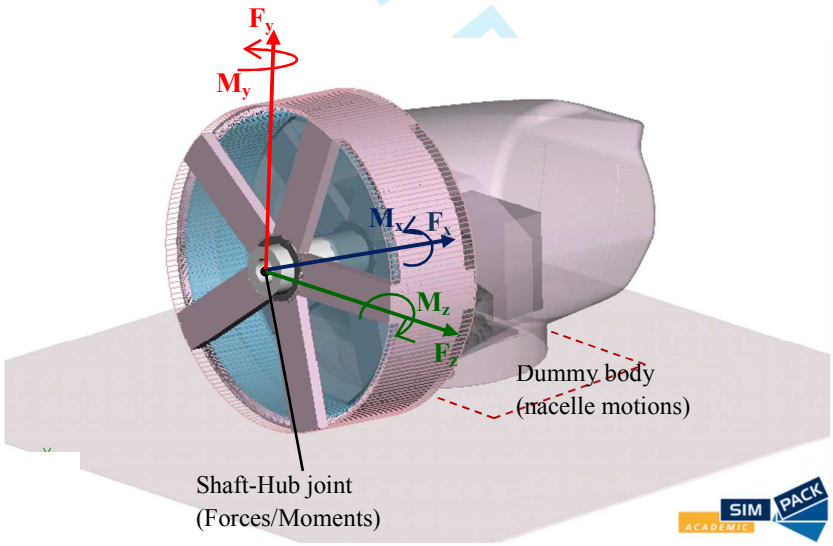

Fig. 9 Shaft loads, moments and nacelle motions applied to the Stand-alone SIMPACK model

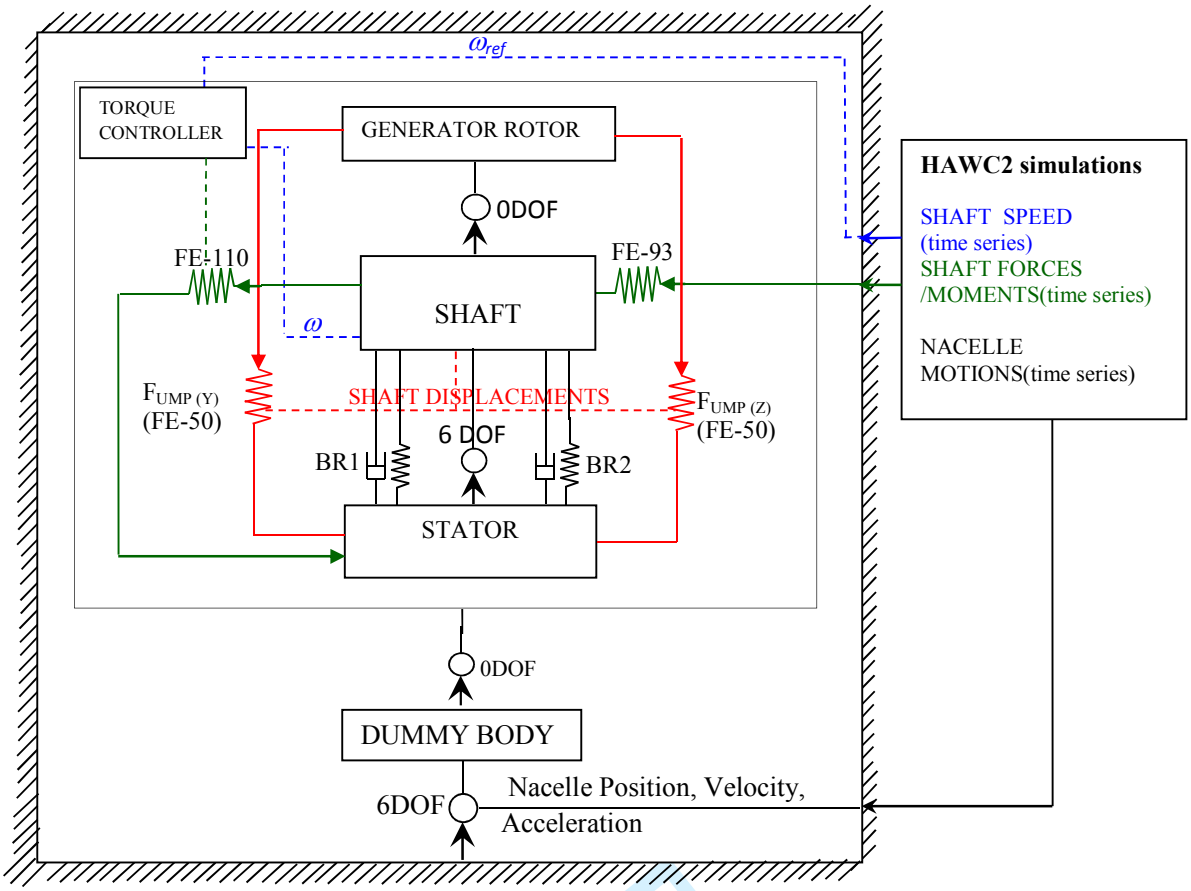

Fig. 10 SIMPACK topology diagram for WTDD and FWTDD analysis

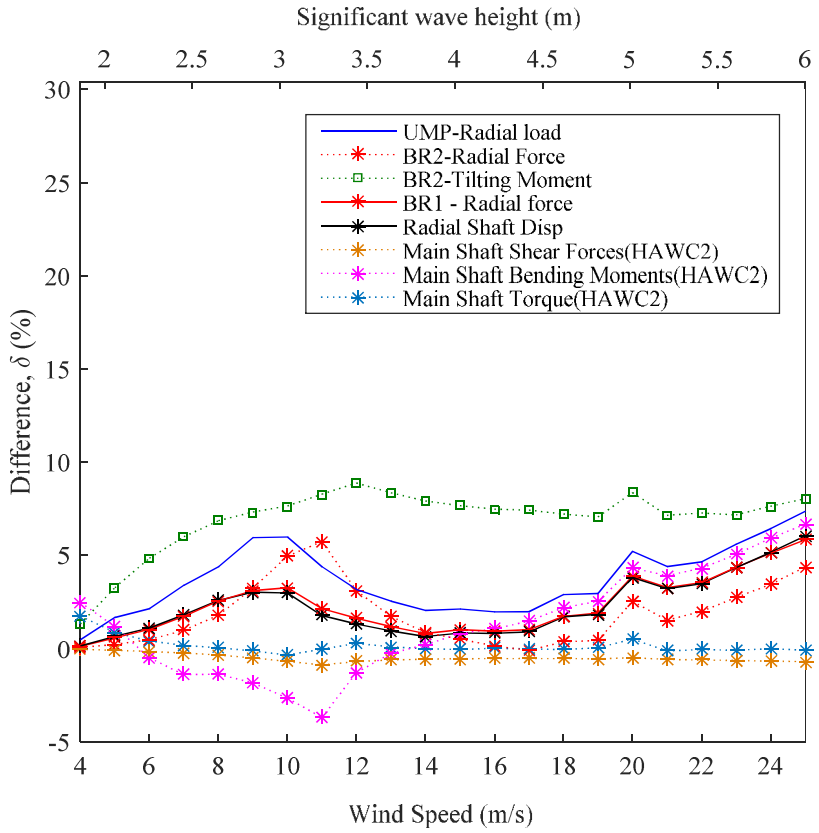

(a)

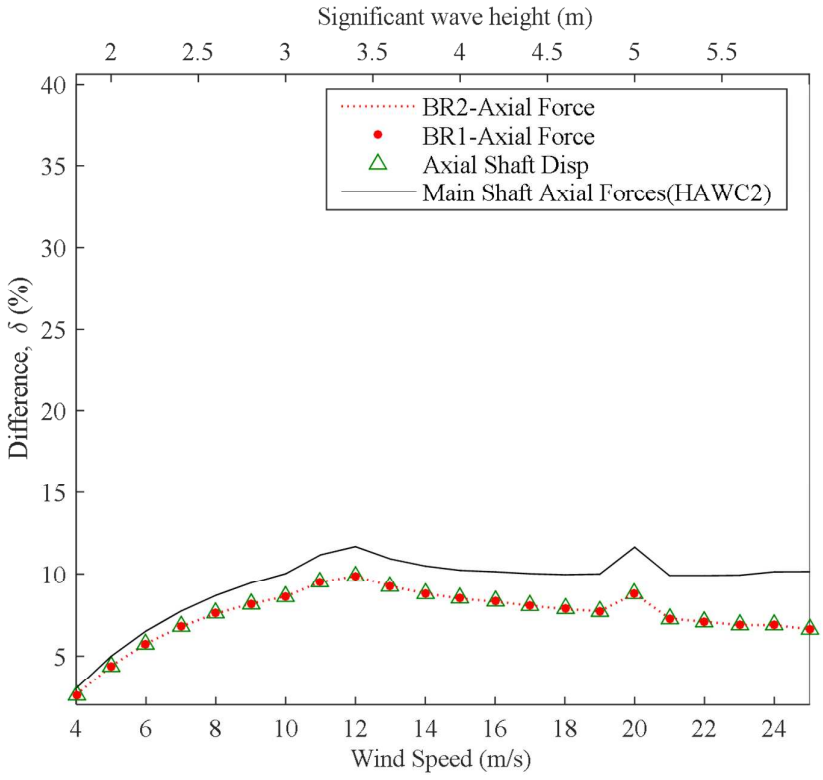

(b)

Fig. 11 Internal drive-train response-Mean Values: FWTDD Vs WTDD (a) Radial and Tilt responses (b) Axial responses

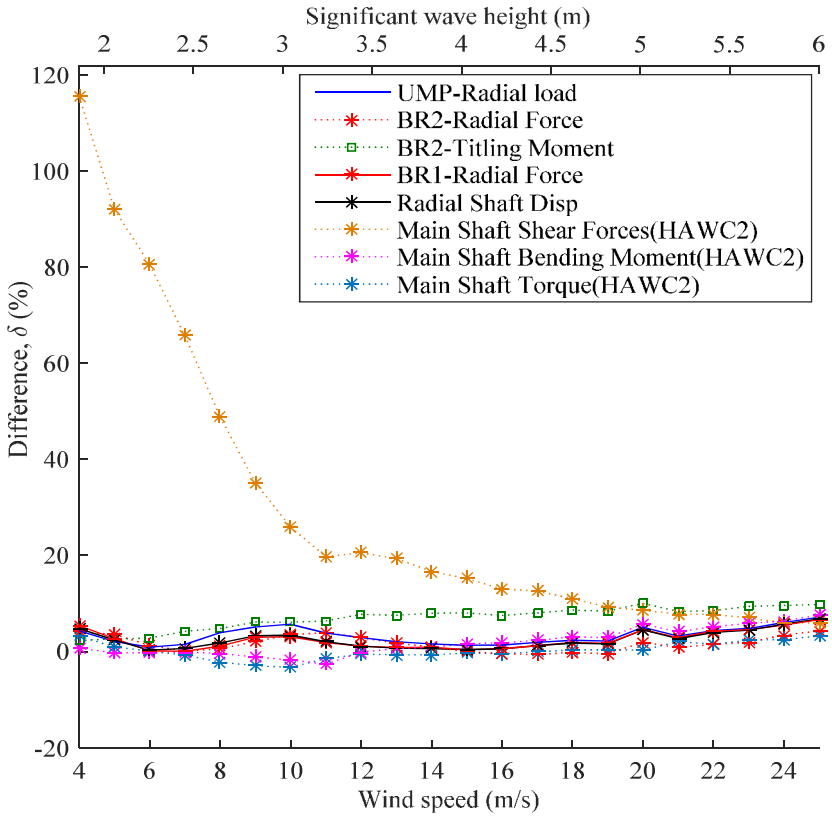

(a)

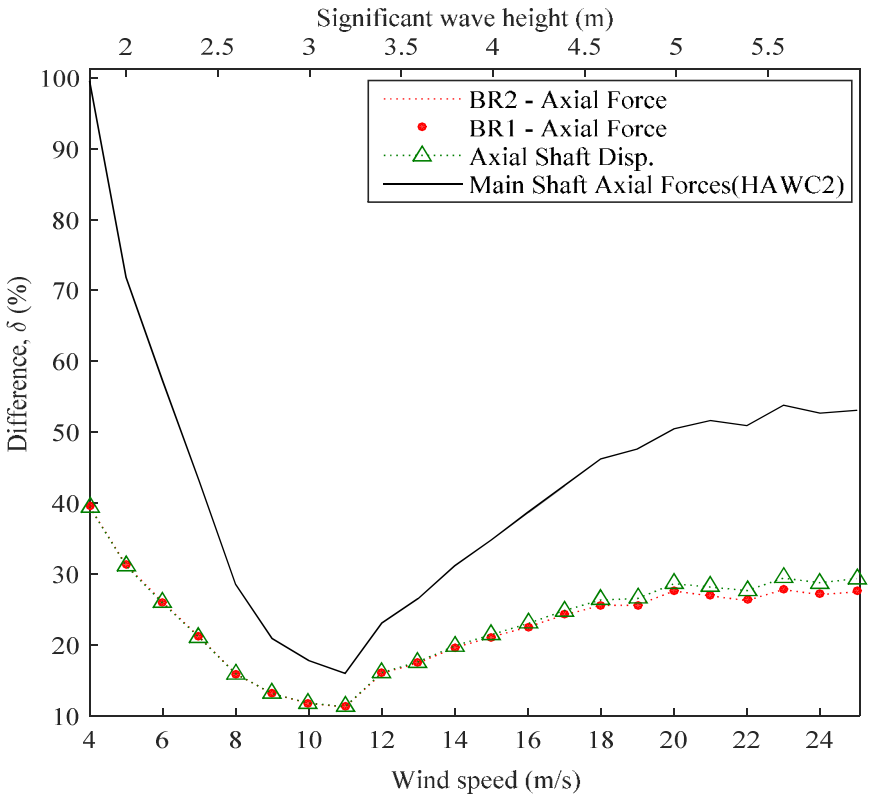

(b)

Fig. 12 Internal drive-train response-Standard Deviation: FWTDD Vs WTDD (a) Radial and Tilt responses (b) Axial responses

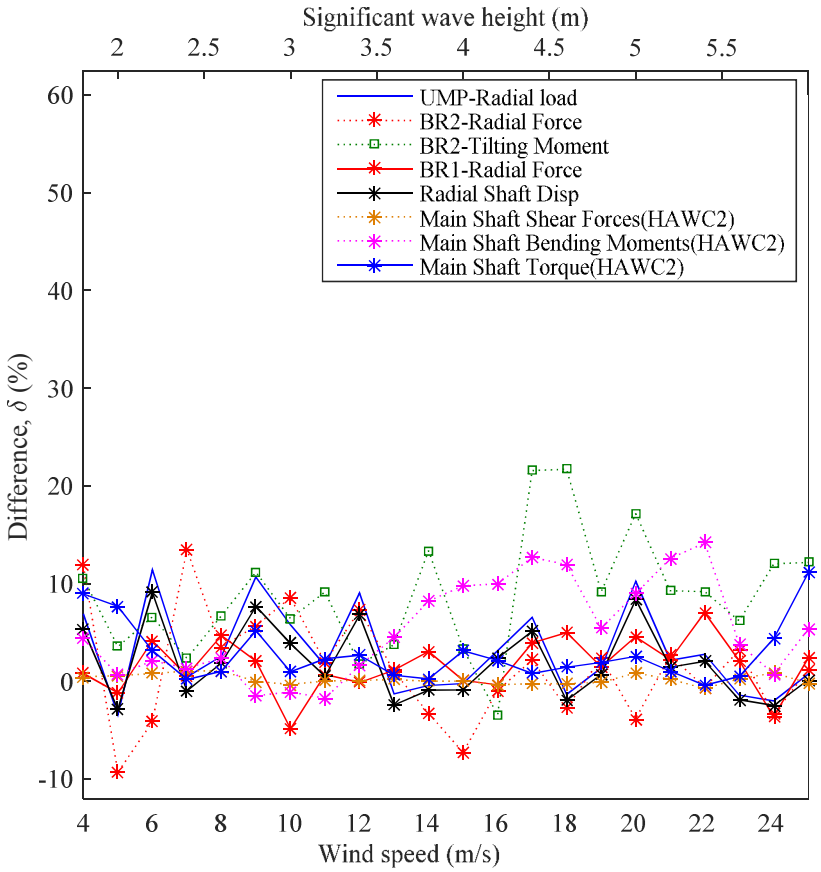

(a)

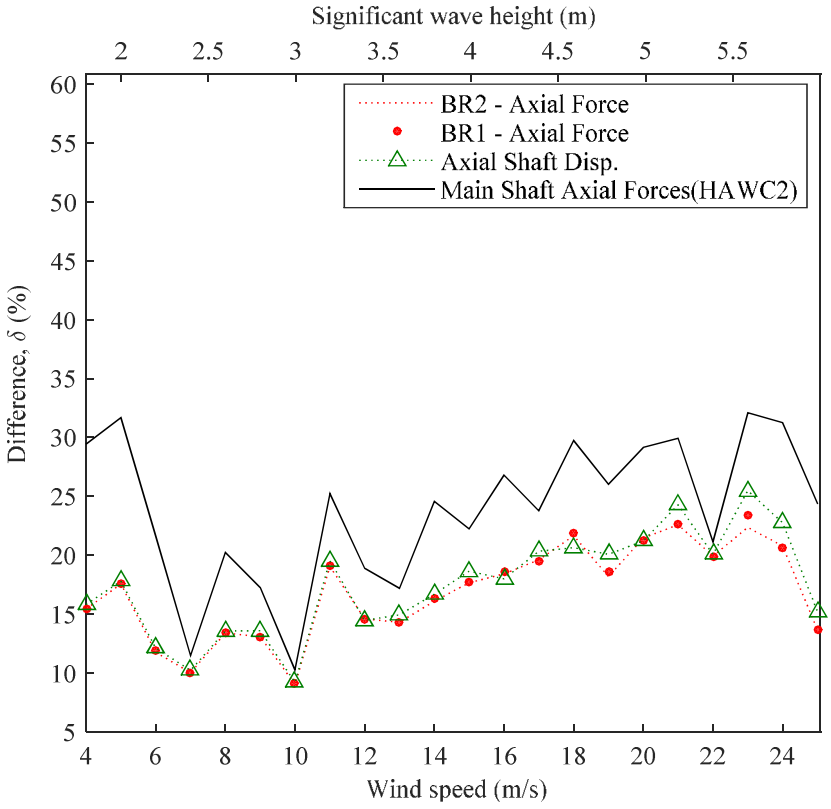

(b)

Fig. 13 Internal drive-train response- Maximum Values: FWTDD Vs WTDD
(a) Radial and Tilt responses (b) Axial responses

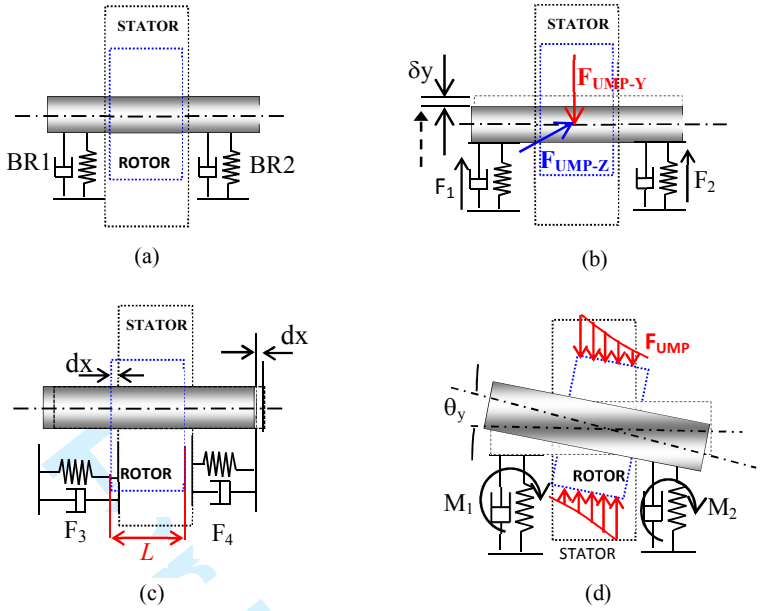

Fig. 14 Shaft displacements and UMP based on [6] (a) Concentric rotor (b) Radial displacement (c) Axial displacement (d) Tilt displacement(Y-axis)

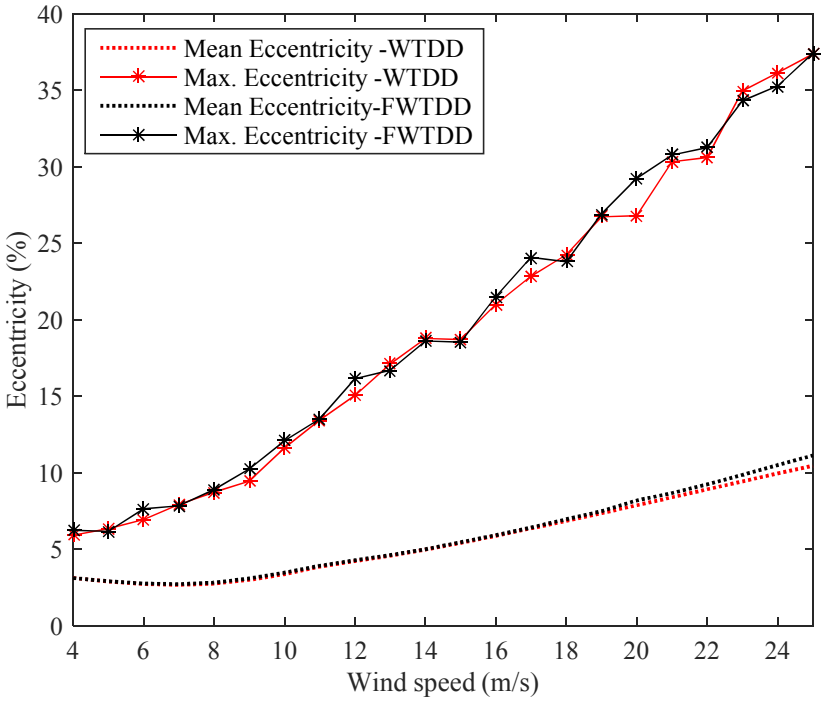

Fig. 15 Eccentricity (%) for different wind speeds for WTDD and FWTDD system

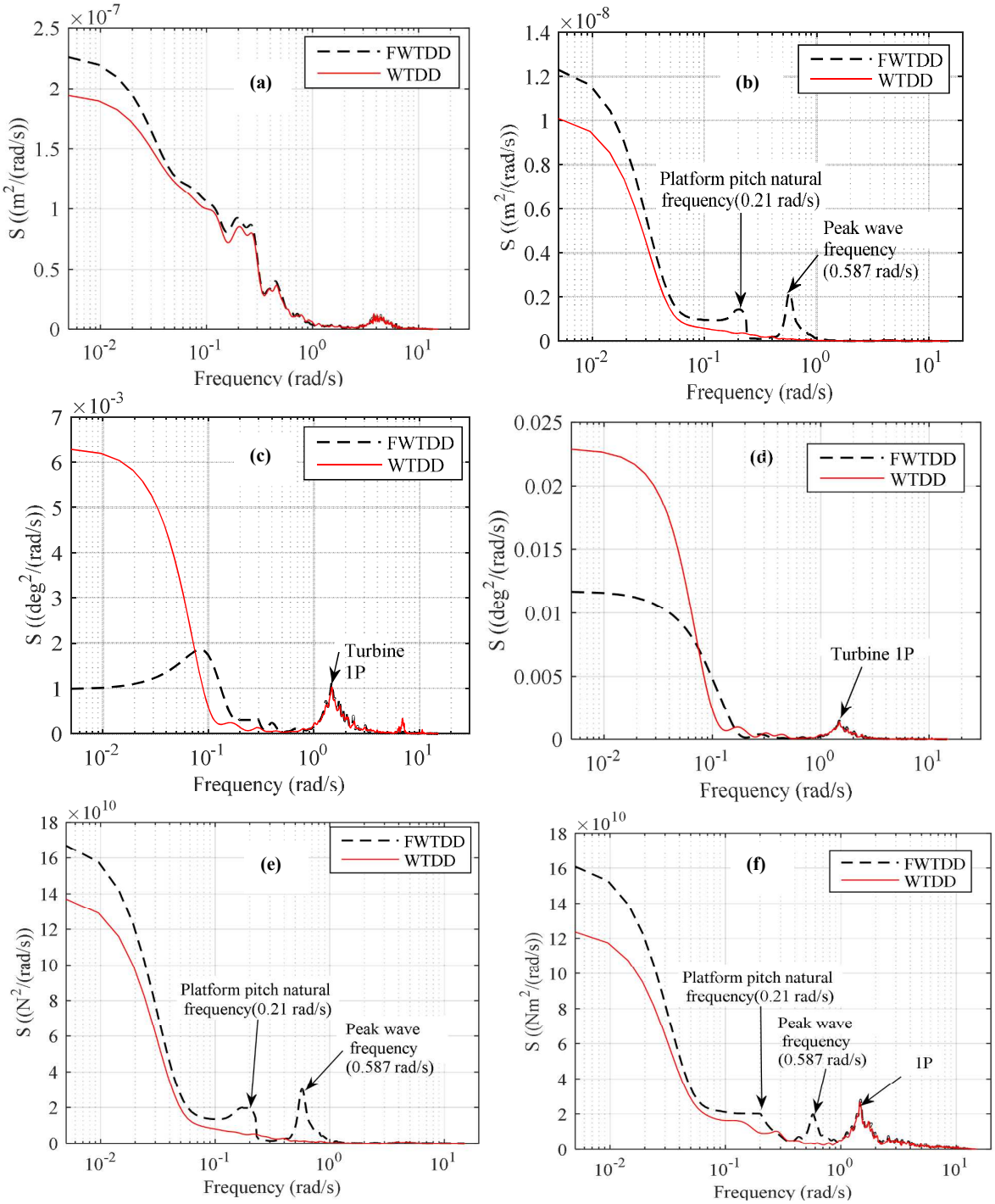

Fig. 16 Spectral density function (a) Radial displacement (b) Axial displacement (c) Tilt displacement(θ_y) (d) Tilt displacement (θ_z) (e) BR2 axial forces (f) BR2 bending moment

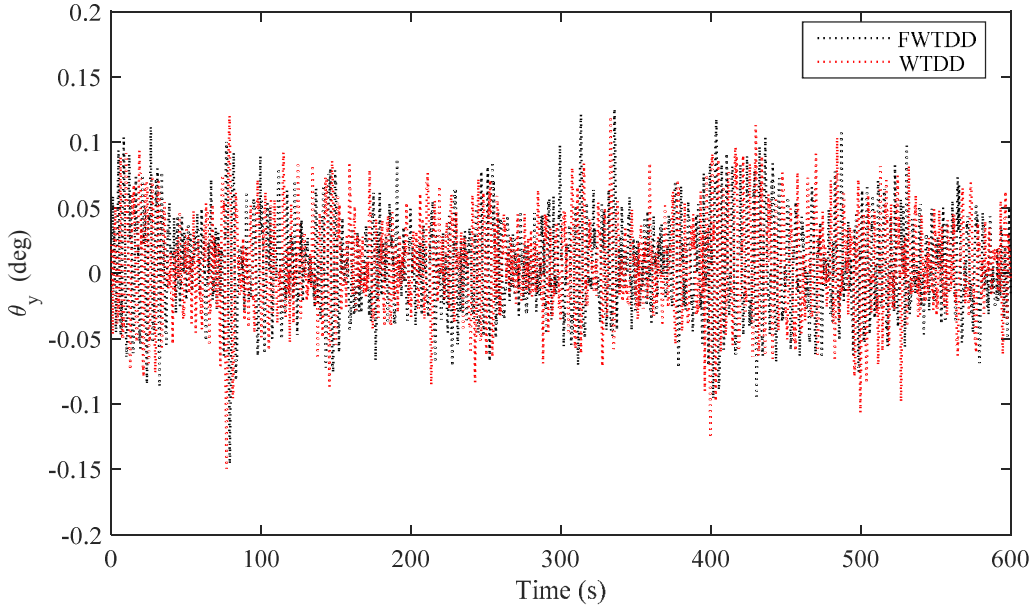

(a)

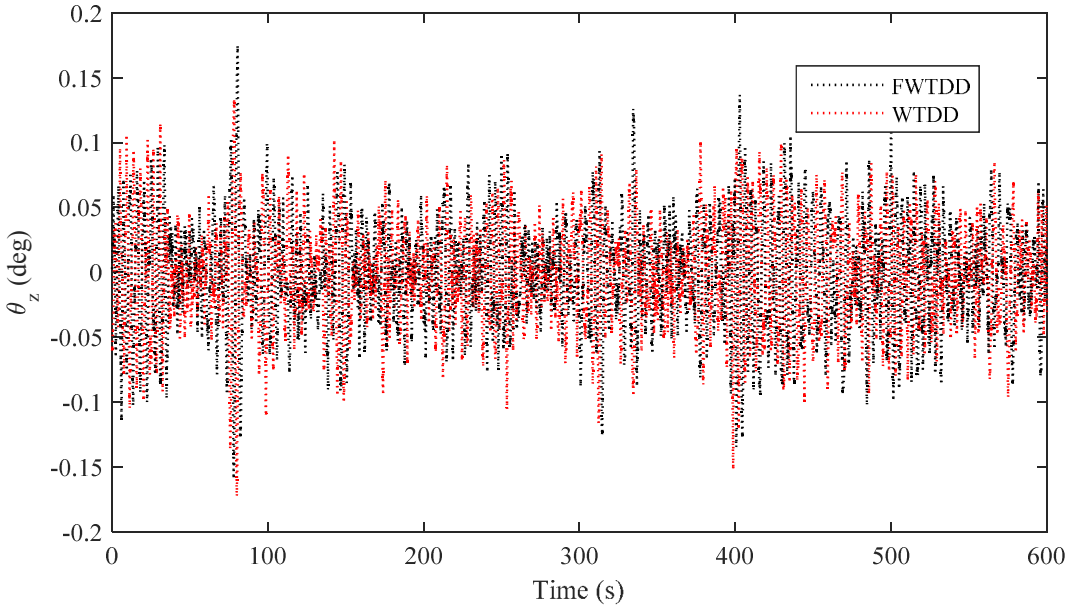

(b)

Fig. 17 Main Shaft Tilt displacement history for a wind speed of 25m/s
(a) Pitch angle(θ_y) (b) Yaw angle (θ_z)

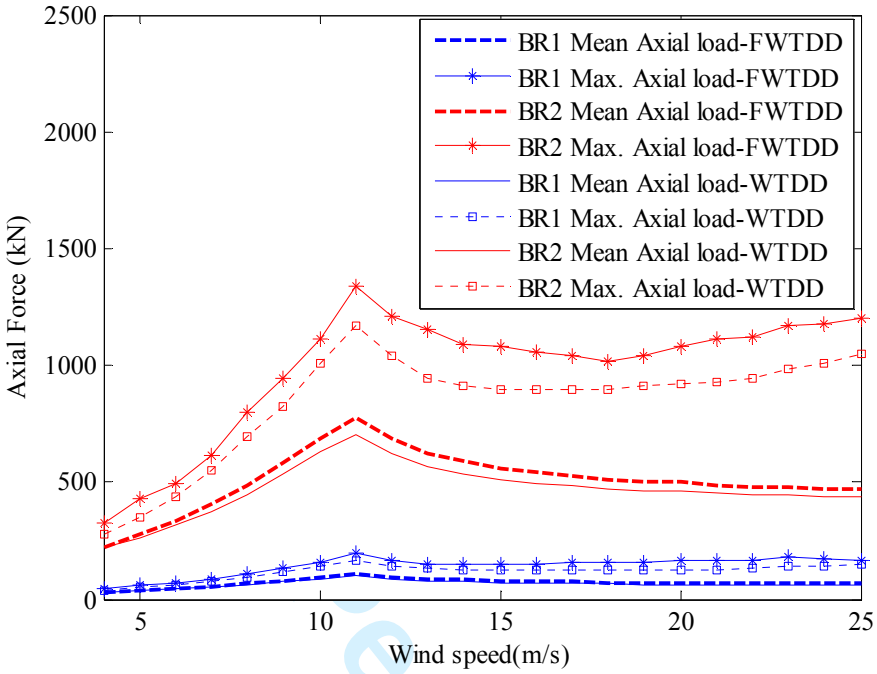

Fig. 18 Bearing axial loads at different wind speeds for FWTDD and WTDD systems

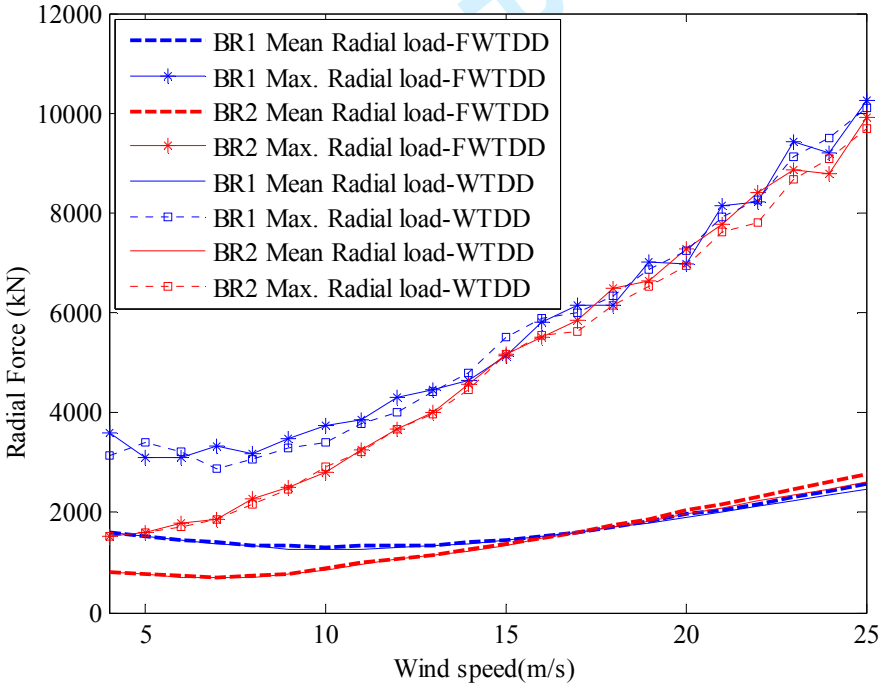

Fig. 19 Bearing radial loads at different wind speeds for FWTDD and WTDD systems

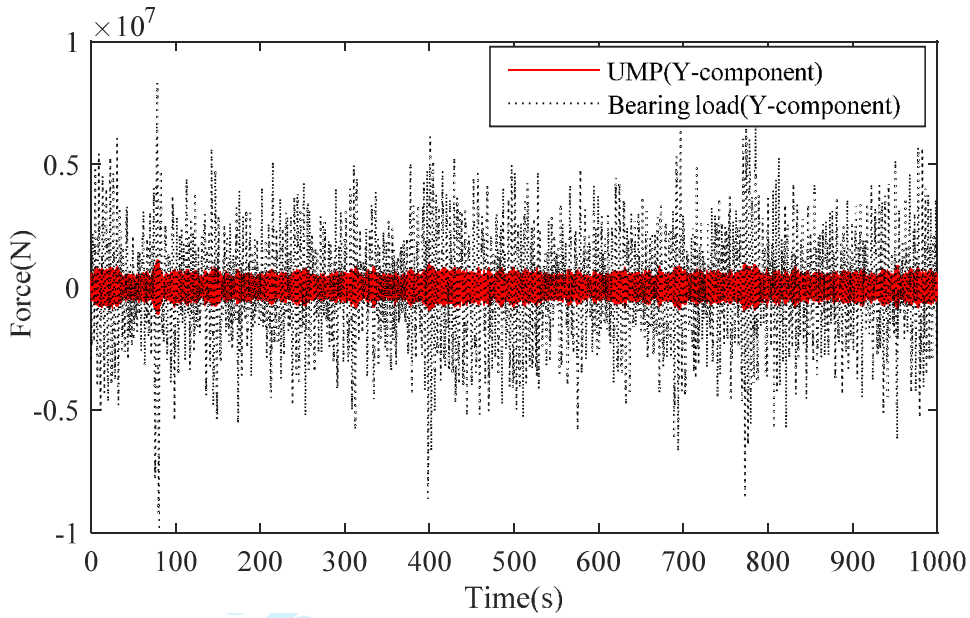

Fig. 20 Time histories of bearing radial load (BR2) and forces due to UMP

Generator rotor diameter	D_g	6360
Axial length	l	1720
Air gap length	g	6.36
Magnet height	l_m	15.9
Stator diameter	D_s	6370
Number of phases	m	3
Stator slot pitch	τ_s	33
Number of slots /pole/ phase	q	1
Pole pitch	τ_p	100
Number of pole pairs	p	100
Rotor pole width	b_p	80
Stator slot width	b_s	15
Stator tooth width	b_t	18
Stator slot height	h_s	80
Stator yoke height	h_{sy}	40
Rotor yoke height	h_{ry}	40
Nominal current,[A]	I_{nom}	606.2
Number of conductors per slot	N_{cslot}	3.35
Peak flux density in the air-gap,[T]	$\widehat{B}_g$	0.97
RMS value of no-load voltage,[kV]	E	3.05
Force density, [kN/m^2]	F_d	40

Table 1. Generator design data and dimensions (in mm)[22]

Control Region	Generator Demand Torque
i	T_{Gen}(i)
1	0
1-1/2	(10.155Ω-7 .3319) 10^6
2	$\left(\frac{\pi}{30}\right)K_T\Omega^2$
2-1/2	(12 .032 Ω- 10 .866)10^6
3	$\left(\frac{P_0}{\Omega}\right)$

Table 2. Turbine Control laws[6]

Natural mode description	Natural frequency (rad/s)	Natural frequencies for different bearing compliances (rad/s)		
		Case I	Case II	Case III
Turbine 1P	1.56	-	-	-
Torsional rigid body	75.39	-	-	-
X-axial	100.53	-	-	-
Z-direction tilting(driven end)	119.38	-	-	-
Y-direction tilting(driven end)	125.66	-	-	-
Z-direction transverse(driven end)	728.80	652.13	631.49	622.82
Y-direction transverse(driven end)	728.85	651.90	631.23	620.58

Table 3 . Drive-train natural modes and frequencies

Item/description	Units	FWTDD system
Turbine power	MW	5
Rated rotor speed	rpm	12.1
Rated generator speed	rpm	12.1
Generator rated Torque	MN-m	4.3
Cut-in,rated,cut-out wind speed	$m\text{-}s^{-1}$	3,11.4,25
Control	-	Variable speed, collective pitch
Generator Efficiency	%	96.6
Generator Inertia about low speed shaft	$kg\text{-}m^2$	$3.79x10^5$
Turbine Inertia about low speed shaft	$kg\text{-}m^2$	$3.54\ x10^7$
Equivalent torsional stiffness of drive-shaft	$Nm\text{-}rad^{-1}$	$2.17x10^9$
Equivalent torsional damping of drive-shaft	$Nms\text{-}rad^{-1}$	$2.85\ x10^6$

Table 4. Main specifications of the FWTDD system